

Spring 2015

## **Micro-Computed Tomography-Based Finite Element Analysis Of The Mechanical Integrity Of In Vivo Biodegradable Magnesium-Alloy Screw And Surrounding Bone**

Adrienne F.O. Williams  
*North Carolina Agricultural and Technical State University*

Follow this and additional works at: <https://digital.library.ncat.edu/theses>

---

### **Recommended Citation**

Williams, Adrienne F.O., "Micro-Computed Tomography-Based Finite Element Analysis Of The Mechanical Integrity Of In Vivo Biodegradable Magnesium-Alloy Screw And Surrounding Bone" (2015). *Theses*. 261. <https://digital.library.ncat.edu/theses/261>

This Thesis is brought to you for free and open access by the Electronic Theses and Dissertations at Aggie Digital Collections and Scholarship. It has been accepted for inclusion in Theses by an authorized administrator of Aggie Digital Collections and Scholarship. For more information, please contact [iyanna@ncat.edu](mailto:iyanna@ncat.edu).

Micro-Computed Tomography-based Finite Element Analysis of the Mechanical Integrity of *In Vivo* Biodegradable Magnesium-alloy Screw and Surrounding Bone

Adrienne F.O. Williams

North Carolina A&T State University

A thesis submitted to the graduate faculty  
in partial fulfillment of the requirements for the degree of

MASTER OF SCIENCE

Department: Chemical, Biological & Bioengineering

Major: Bioengineering

Major Professor: Dr. Matthew B.A. McCullough

Greensboro, North Carolina

2015

The Graduate School  
North Carolina Agricultural and Technical State University

This is to certify that the Master's Thesis of

Adrienne F.O. Williams

has met the thesis requirements of  
North Carolina Agricultural and Technical State University

Greensboro, North Carolina  
2015

Approved by:

---

Dr. Matthew B.A. McCullough  
Major Professor

---

Dr. Narayan Bhattarai  
Committee Member

---

Dr. DeRome Dunn  
Committee Member

---

Dr. Stephen B. Knisley  
Department Chair

---

Dr. Sanjiv Sarin  
Dean, The Graduate School

© Copyright by  
Adrienne F.O. Williams  
2015

### Biographical Sketch

Adrienne F.O. Williams was born on January 24, 1992, in London, England. She completed her Bachelor of Science degree in Medical Physics with a double minor in Alternative Energy and Spanish from The University of the West Indies, Mona, Kingston, Jamaica in 2013. Immediately after her undergraduate studies, she joined the Master of Science program in Bioengineering at North Carolina A&T State University. As a graduate student at North Carolina A&T she made research contributions as a part of the National Science Foundation funded Engineering Research Center for Revolutionizing Metallic Biomaterials (NSF ERC-RMB) and Dr Matthew McCullough's Biomechanics lab group along with contributions to her department as a Teaching Assistant. After obtaining her Master's degree, she will pursue a Doctorate in Biomedical Engineering.

## Acknowledgments

“...To God be the glory, great things He has done!”

To my advisor, Dr. McCullough: Thank you for your guidance and support which made this work possible. To Dr. Boyce Collins, thank you for training me to use the micro-CT machine and for your encouragement of my research. To my research colleagues, Ashley and Robert: I am very thankful for the time and support extended to me during our labor together. I am also truly thankful to the Metropolitan United Methodist church community, the Jamaican Association of Greensboro, my Professors, especially Dr Knisley and Mr Alford, and the Administrative staff in the ERC and CBBE Department, especially Mrs Lois Dalton Deve, Ms Armelia McLaughlin and Ms Courtney Chavis, who have made my learning experience in Greensboro easier and more fruitful through their support, well wishes and love. Finally, I thank my family for their eternal support, my mum, dad, brother, and wonderful husband, a big Thank You. Also, I couldn't ask for better support from Granddad, both my Grandmas, Aunty Sharon and Aunty Maureen. Thank you for being a part of my continued journey. I appreciate you all!

## Table of Contents

List of Figures .....	x
List of Tables .....	xii
Abstract .....	1
CHAPTER 1 Introduction.....	2
1.1 Background.....	2
1.2 Problem Statement.....	2
1.3 Objectives .....	3
1.4 Hypothesis .....	3
CHAPTER 2 Literature Review .....	4
2.1 Bone.....	4
2.1.1 Introduction. ....	4
2.1.2 Types of bone tissue. ....	4
2.1.3 Anatomy and physiology of long bones. ....	5
2.1.4 Material and mechanical properties of bone. ....	6
2.1.5 Bone healing and remodeling. ....	7
2.1.6 Imaging bone .....	8
2.1.6.1 Radiography. ....	8
2.1.6.2 X-ray Computed Tomography (CT). ....	8
2.2 Orthopedic Biomaterials and Devices .....	9
2.2.1 Introduction. ....	9
2.2.2 Non-degradable/Permanent Orthopedic Implants. ....	10
2.2.2.1 Metals. ....	10
2.2.2.2 Ceramics.....	12

2.2.2.3 Composites.....	12
2.2.3 Biodegradable Orthopedic Implants.....	12
2.2.3.1 Ceramics.....	12
2.2.3.2 Polymers/Plastics.....	13
2.2.3.3 Magnesium and its alloys.....	13
2.3 In Vivo Performance of Orthopedic Biomaterials (Focused on Screws and Plates).....	15
2.3.1 Biological performance.....	15
2.3.2 Mechanical Performance.....	17
2.4 Mechanical Testing of Biomaterials and Orthopedic Devices.....	18
2.4.1 Introduction.....	18
2.4.2 Destructive and proof testing.....	18
2.4.2.1 Universal testing machines (UTMs).....	18
2.4.3 Non-destructive testing.....	19
2.4.4 Testing Methods.....	19
2.4.4.1 Nanoindentation and Atomic Force Microscopy (AFM).....	19
2.5 Introduction to Finite Element Analysis.....	20
2.5.1 Introduction.....	20
2.6 CT to FEA for Orthopedic Applications.....	21
2.6.1 Introduction.....	21
2.6.2 General method for CT to FEA studies.....	21
2.6.3 CT to FEA studies of bone.....	22
2.6.3.1 Ex vivo studies.....	22
2.6.3.2 In vivo studies.....	23
2.6.4 CT to FEA of <i>in vivo</i> magnesium devices.....	23

CHAPTER 3 Methodology.....	26
3.1 Micro-Computed Tomography to Finite Element Analysis Study.....	26
3.1.1 Samples.....	26
3.1.2 Micro-CT scan acquisition. ....	26
3.1.3 Micro-CT reconstruction and data processing. ....	27
3.1.4 3-D Volume segmentation.....	28
3.1.5 Material property assignment. ....	30
3.1.6 Meshing.....	31
3.1.6.1 Mimics.....	31
3.1.6.2 3-matic.....	32
3.1.7 Finite Element Analysis (FEA). ....	33
3.2 FEA of Screw in Woven Bone .....	33
3.2.1 3D CAD Model. ....	33
3.2.2 Material Properties. ....	34
3.2.3 Finite Element Analysis .....	35
3.2.3.1 Finite Element Software.....	35
3.2.3.2 Meshing and convergence. ....	35
3.2.3.3 Model Validation.....	36
3.2.4 Simulation.....	36
3.2.4.1 Models.....	36
3.2.4.2 Boundary conditions. ....	37
3.2.5 Analysis. ....	38
CHAPTER 4 Results.....	39
4.1 Micro-CT to Finite Element Analysis .....	39
4.1.1 Meshing in Mimics and 3-Matic. ....	39

4.1.1.1 Mimics.....	39
4.1.1.2 Meshing in 3-Matic. ....	40
4.1.2 Finite Element Analysis Job.....	41
4.2 FEA of Screw in Woven Bone .....	43
4.2.1 Meshing .....	43
4.2.2 Output.....	43
CHAPTER 5 Discussion and Future Research.....	49
5.1 Micro-CT to Finite Element Analysis .....	49
5.1.1 3-D volume segmentation.....	49
5.1.2 Material property assignment.....	50
5.1.3 Meshing in Mimics and 3-Matic .....	50
5.1.3.1 Meshing in Mimics.....	50
5.1.3.2 Meshing in 3-Matic. ....	51
5.1.4 Finite Element Analysis. ....	51
5.2 FEA of Screw in Woven Bone .....	52
5.2.1 Model creation.....	52
5.2.2 Meshing.....	52
5.2.3 Analysis and Output.....	52
5.3 Limitations.....	53
5.4 Future Work.....	54
5.5 Conclusions.....	54
References.....	56

## List of Figures

Figure 1. The structure of a femur (Ogele, 2013). .....	6
Figure 2. Diagram of a finite element model with a finite number of discretized elements and nodes, as well as boundary conditions (E. F. Morgan & Bouxsein, 2005).....	21
Figure 3. CT to FEA process of an implant-bone-compound (Kluess, 2010). .....	24
Figure 4. The Nanotom M micro-CT machine setup, with mounted 2B pencil. ....	27
Figure 5. Segmented masks in of the $\mu$ -CT data in Mimics. ....	30
Figure 6. Material property assignment tab in Mimics with histogram of Hounsfield units in a model.....	31
Figure 7. Flow chart of $\mu$ -CT to FEA protocol used. ....	32
Figure 8. CAD drawing of the original baseline Generation One Johnson and Johnson screw design (Hawkins, 2013). ....	34
Figure 9. A wire-frame rendered model of the mesh and nodes of the model. ....	36
Figure 10. Boundary conditions used in the finite element models.....	37
Figure 11. The volume meshing options in Mimics. ....	39
Figure 12. Hexahedral (8-node) mesh of about 36,000 elements created by Mimics but imported into Abaqus. ....	41
Figure 13. Flow chart of $\mu$ -CT to FEA protocol used with the file types obtained at each step. .	42
Figure 14. Bar chart of the maximum reaction force results of the FEA models. ....	44
Figure 15. Bar chart of the maximum displacement results of the FEA models. ....	45
Figure 16. Comparison of the magnitudes of the reaction forces (RF) that occurred when the magnesium-alloy (left) and the PLLA:PLGA copolymer (right) underwent the same axial pull-out test in woven bone with a maximum elastic modulus. ....	46

Figure 17. Comparison of the translation (UT) that occurred when the magnesium-alloy (left) and the PLLA:PLGA copolymer (right) underwent the same axial pull-out test in woven bone with a maximum elastic modulus. ....	47
Figure 18. Comparison of the translation magnitude (UT) and the translation in the vertical direction (UT2) that occurred when the PLLA:PLGA copolymer (left and right) underwent pull-out testing in woven bone with a maximum elastic modulus. ....	48

## List of Tables

Table 1 Materials for use in the body (Park & Bronzino, 2002). .....	9
Table 2 Summary of the physical and mechanical properties of various implant materials in comparison to natural bone (Staiger et al., 2006) .....	14
Table 3 Information on the DICOM image stacks from micro-CT scans. ....	28
Table 4 Masks of the scan components created in Mimics by thresholding .....	29
Table 5 Material properties assigned to the bone, Mg-alloy screw and PLLA:PLGA screw in the FE models .....	35
Table 6 Basic characteristics of the volume meshes of the in vivo device generated in 3-matic.	40
Table 7 Maximum reaction force values obtained from FEA of each model.....	44
Table 8 Maximum displacement values obtained from FEA of each model.....	45

## Abstract

The anterior cruciate ligament (ACL) tear, the most common knee injury, affects 100,000 to 200,000 persons in the US annually. Surgical repair is employed to restore the knee to its full range of motion. In the surgery, an interference screw is used to secure a soft tissue graft that is used to replace the torn ACL. In 2012, orthopedic devices for knees accounted for the largest share of the \$29.2 billion overall revenue for orthopedic devices. Biodegradable implants are expected to lead growth in the orthopedic sector by increasing the quality of life and decreasing recovery time after orthopedic injury for athletes and non-athletes and aging, osteoporotic, osteoarthritic and obese populations. Magnesium-based orthopedic devices, including interference screws, are being investigated because of their ability to provide high strength as a metal, but degrade like a polymer.

One objective of this study was to compare the pull-out forces of an unnamed magnesium-alloy against a commercially available copolymer, 82:18 PLLA:PLGA, in woven bone using finite element analysis. The reaction forces in bone and displacement of the screws were used to assess the overall performance of each material in a pull-out test. The second objective of this work was to develop and evaluate micro-computed tomography-based finite element models of *in vivo* biodegradable screws of the unnamed magnesium-alloy over time in rabbit femurs.

Several foundational observations were made about modeling *in vivo* degrading magnesium devices with a micro-CT to FEA protocol. The results of this work have shown that an unnamed biodegradable magnesium-alloy and a biodegradable 82:18 PLLA:PLGA copolymer performed equally in nodal displacement and that the Mg-based device only outperformed the copolymer in  $E_{\min}$  woven bone.

## **CHAPTER 1**

### **Introduction**

#### **1.1 Background**

The global market for orthopedic devices is expected to grow to \$41.2 billion by 2019. In 2012, orthopedics devices for knees accounted for the largest share of the \$29.2 billion overall revenue (Parmar, 2014). The most common contact and non-contact knee injury is the anterior cruciate ligament (ACL) tear, which affects 100,000 to 200,000 persons in the US annually. Surgical repair is employed to restore the knee to its full range of motion. In this arthroscopic surgery, a hamstring or patellar tendon autograft is used to replace the torn ACL and secured with staples or interference screws made of suitable biomaterials (D. G. Morgan, 2015).

#### **1.2 Problem Statement**

Traditionally, these biomaterials have been metals such as titanium and its alloys, stainless steels and cobalt-chromium. These metals provide excellent fixation strength, but are so strong that they absorb stresses that would normally dissipate into the bone, causing bone resorption (since the bone is not being loaded) and subsequent implant loosening. Metallic interference screws and orthopedic devices are permanent and therefore require revision surgeries, which cost the patient and increase their recovery time. Biodegradable materials have eliminated the need for revision surgeries. Biodegradable implants are expected to lead growth in the orthopedic sector by increasing the quality of life and decreasing recovery time after orthopedic injury for athletes and non-athletes and aging, osteoporotic, osteoarthritic and obese populations. Commercially available biodegradable polymers show good biocompatibility, but are not strong enough for many orthopedic applications. Magnesium (Mg) and its alloys, on the other hand, are an attractive group of biomaterials for orthopedics because of their degradability

and their mechanical properties, which are close to bone and best suited for orthopedic implants such as ACL screws. Their ability to provide mechanical strength is similar to bone which allows for superior bone healing- as opposed to softer non-metallic biodegradable materials. Characterizing the mechanical changes and interactions of these promising degradable Mg and Mg-alloy biomaterials and the host environment (bone) is essential to their success and application in orthopedic devices.

### **1.3 Objectives**

The overall goal is to determine the mechanical properties of biodegradable magnesium screws and surrounding new bone over time in order to:

- i. Develop a protocol to create 3D finite element models of degradable magnesium screws in bone with corrosion layer, from micro-CT data taken over time.
- ii. Compare the pull-out performance of an unnamed magnesium-alloy screw and a commercially available 82:18 PLLA:PLGA copolymer screw.

### **1.4 Hypothesis**

It is hypothesized that the magnesium-alloy screw will have a stronger pull-out force than a 82:18 PLLA:PLGA copolymer screw.

## CHAPTER 2

### Literature Review

#### 2.1 Bone

**2.1.1 Introduction.** Bone is the main organ of the skeletal system. Bone is a dynamic system that responds to loads by constantly changing its properties. It provides structural support and protection for other organs in the body and enables movement, among other functions such as blood cell production and mineral storage. Bone has a 60% mineral/inorganic composition by weight, of mainly calcium phosphate (with a Ca:P ratio of 1.37-1.87) and small quantities of silicon, potassium carbonate, zinc, strontium, magnesium and chloride or fluoride. The calcium phosphate in bone is seen as an impure form of hydroxyapatite (HA), a naturally occurring ceramic crystalline mineral with chemical formula  $\text{Ca}_{10}(\text{PO}_4)_6(\text{OH})_2$  and Ca:P ratio of 5:3 or 1.67 (McCloskey & Furnival, 2011). Bone's organic phase accounts for 30% of its weight and consists of collagen and other proteins while water makes the remaining 10% of bone by weight (Al-Sanabani, Madfa, & Al-Sanabani, 2013; Bartel, Davy, & Keaveny, 2006; Keaveny, Morgan, & Yeh, 2003).

**2.1.2 Types of bone tissue.** The two basic types of bone tissue are cortical (or compact) and cancellous (trabecular or spongy). Cancellous bone is the highly porous (50-95% porous by volume), irregularly shaped trabecular structure located in the center of the bone cavity. It can be found at the ends or epiphyses of long bones and in the vertebrae, skull, pelvis and sternum. Cortical bone surrounds cancellous bone and is much denser, with only about 30% porosity (ranges from 5%-30% porous by volume, with age) which is not visible to the naked eye. It is found in the diaphysis or shaft of long bones like the femur and tibia. After bone damage, collagen becomes mineralized leading to the formation new bone, a third type of bone tissue.

New bone takes a stacked or lamellar form in adults, or a randomly oriented or woven form during stages of rapid bone growth seen commonly in children, large animals, or in the initial healing period after a fracture. Lamellar bone layers tend to form Haversian systems and become cortical bone, while cancellous bone is formed by bone cells called osteoblasts which deposit new bone in a less organized method (Bartel et al., 2006; Keaveny et al., 2003).

**2.1.3 Anatomy and physiology of long bones.** Long bones (Figure 1) are the tubular bones of the extremities and they have three main structural sections. The tubular diaphysis grows from its end plates or epiphyseal plates, which close upon maturation of the individual and become the epiphyseal line or scar. The large ends of long bones, called the epiphyses, grow from separate ossification centers. The metaphysis is the region of bone between the diaphysis and the epiphysis. The inner surface of the bone is called the endosteum and the periosteum is a fibrous membrane that covers the outer or periosteal surface. Other parts of the bone tend to have physiological function only and no structural function. For example, medullary or marrow cavity contains yellow marrow made primarily of fat and few blood cells and red marrow (where red blood cells are made) is found in cancellous bone the proximal ends of the humerus and femur. Arteries are interspersed throughout the periosteum, medullary cavity and epiphyses to provide a blood supply (Bartel et al., 2006).

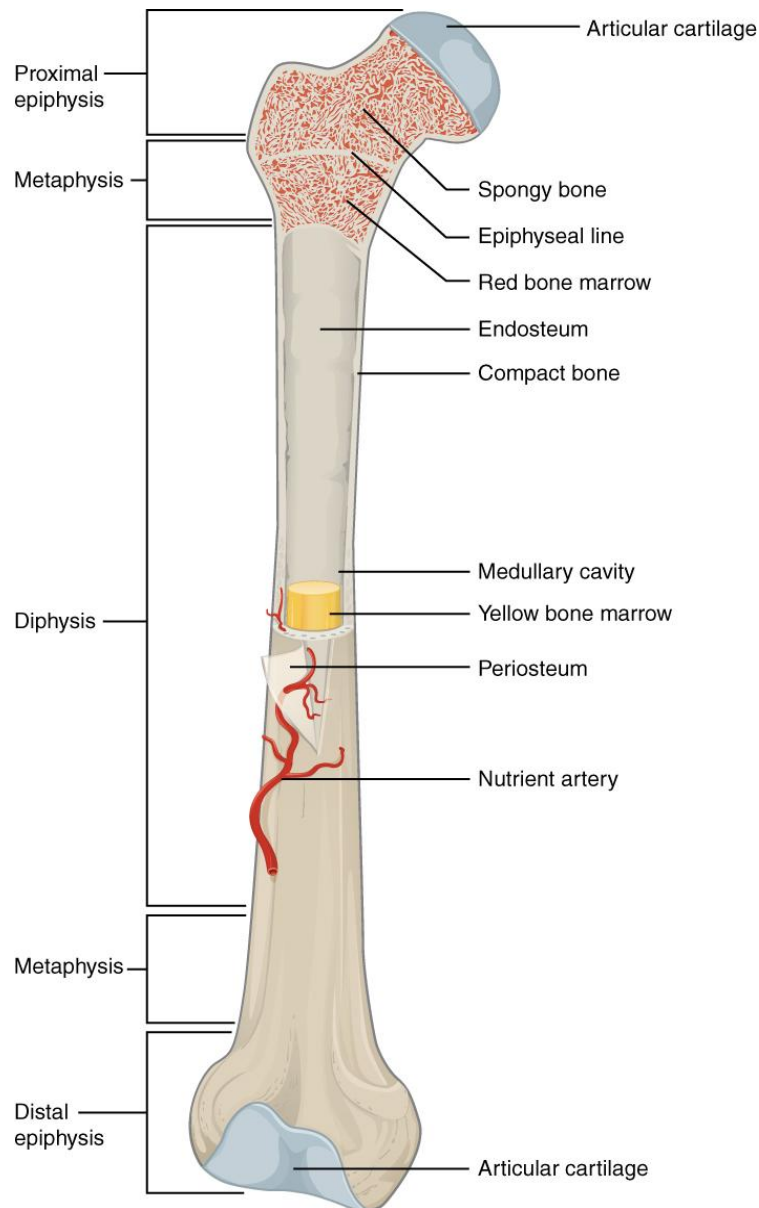


*Figure 1. The structure of a femur (Ogele, 2013).*

**2.1.4 Material and mechanical properties of bone.** Bone is heterogeneous because its material properties such as density and porosity vary with spatial and anatomical location, age and health. The inorganic to organic content ratio of bone affects its mechanical properties. Bone is also anisotropic meaning that its material properties are dependent on the direction in which the load is applied. Cortical bone is transversely isotropic since its longitudinal (or primary) direction has different properties from its isotropic transverse plane which is

perpendicular. It is stronger and stiffer in the longitudinal direction (than transverse direction) or along the length of the bone and is stronger in compression than in tension. The longitudinal elastic or Young's modulus of cortical bone has a wide range from 10-22 GPa because of its age-dependent, variable porosity and strength to modulus ratios of 1.12% and 0.78% for longitudinal tension and compression respectively (Bartel et al., 2006). Trabecular bone, also anisotropic, has elastic moduli ranging from 10-3000 MPa which can vary 3- to 100-fold within an anatomic site, because of its large variation in porosity combined with the effects of the direction of load. The strength of trabecular bone ranges from 0.1-30 MPa (Bartel et al., 2006; Chaffin, Andersson, & Martin, 2006; Keaveny et al., 2003).

Long bones are thought to be optimal for the mechanical and structural functions that they perform. For example, the thicknesses of cortical bone in the shafts of long bones are seen as optimal for such a structure with minimum mass. Also, the enlarged epiphyses (with spongy bone inside) are ideal for transmitting large joint loads to cortical bone, which is stiffer and stronger but has a smaller cross-sectional area, without contact pressure (Bartel et al., 2006).

**2.1.5 Bone healing and remodeling.** Bones adapt to their mechanical environment. Therefore the material/mechanical and structural/geometric properties of bone depend on the anatomic site and change with increased or decreased load-bearing, as well as with age and disuse. Bone is anisotropic, meaning that the material properties depend on the direction in which the load is applied. Bone morphology changes over time due to effects of age, genetics and repetitive load-bearing, and bone remodeling constantly occurs to combat these effects (Bartel et al., 2006; Chaffin et al., 2006; Keaveny et al., 2003; Klues, 2010). The dynamic process of bone remodeling involves bone cells called osteoblasts which lay down new bone called woven bone at outer edges of the Haversian canal system, at points of injury or fracture.

Osteocytes are present during mineralization. Gradually, through the parallel arrangement of the collagen fibers and calcium phosphate crystals, the woven bone becomes a more sheet-like lamellar bone. Finally, osteoclasts, perform a reverse process of gradually reabsorbing the bone structure, so that new bone can be laid down. Bone formation and resorption occur simultaneously, especially in adaptive responses to external stressors and forces (Freivalds, 2011). The speed of bone healing/remodeling depends on many factors, including the type of fracture (if applicable), blood supply to the area, exposure to external stimuli, the individual's age and health, including medical conditions and diet. Based on these factors, bone can take between one and six months to heal.

### **2.1.6 Imaging bone**

**2.1.6.1 Radiography.** In radiography, radiation (X-ray, gamma ray, or neutron beam) passes through a sample and is differentially absorbed based on the attenuating properties of the materials such as the thickness, type of material, and the presence of internal flaws or defects. A single 2D image is projected onto a film. Radiography is excellent for imaging bone but causes health concerns for persons because it uses forms of ionizing radiation (Black & Kohser, 2007).

**2.1.6.2 X-ray Computed Tomography (CT).** CT imaging is a more advanced form of radiography and is therefore good for imaging bone but exposes the users and patients to ionizing radiation. It provides a cross-sectional view of the interior of an object along a plane parallel to the X-ray beam. Transmitted x-rays are recorded at each of the numerous detectors while the sample is rotated. Planar images of the interior of the object are reconstructed by complex numerical algorithms (Black & Kohser, 2007). CT images are based on the attenuation of x-rays by the object's features. The attenuation is measured in Hounsfield Units (HU). HUs are normalized in so that air has a value of -1,000 and water has a value of 0. Bone usually has

HU of 250-3,000. Quantitative CT (QCT) is used for non-clinical imaging of large biological samples such long bones. Micro-CT is used for small biological and non-biological samples for which a very high resolution is needed. The DICOM format is the standard CT scan file output.

Like radiography, CT uses ionizing radiation, which is harmful for biological tissues.

## 2.2 Orthopedic Biomaterials and Devices

**2.2.1 Introduction.** A biomaterial may be any material, natural or man-made, that comprises whole or part of a living structure or biomedical device, which performs natural function (Sharma, Sehgal, & Kumar, 2003). Orthopedic biomaterials must always be evaluated for biocompatibility (acceptance in the body)/cytotoxicity, bone response and mechanical stability as well as for biocorrosion and in vivo degradation, if applicable, before they are tested in the body. Biomaterials are used in orthopedic devices to replace diseased or damaged parts such as in artificial hip or knee joints; and to assist in bone healing such as in sutures, bone plates, screws and pins (Table 1) (Park & Bronzino, 2002).

Table 1

*Materials for use in the body (Park & Bronzino, 2002).*

<b>Materials</b>	<b>Advantages</b>	<b>Disadvantages</b>	<b>Examples</b>
<b><i>Polymers</i></b> (nylon, silicone rubber, polyester, polytetrafluoroethylene, etc.)	Resilient Easy to fabricate	Not strong Deforms with time, may degrade	Sutures, blood vessels, hip socket, ear, nose and other soft tissues

Table 1

*Cont.*

<b><i>Metals</i></b> (Ti and its alloys, Co-Cr alloys, stainless steels, Au, Ag, Pt, etc.)	Strong, tough, ductile	May corrode, dense, difficult to make	Joint replacements, bone plates and screws, dental root implants, pacer and suture wires
<b><i>Ceramics</i></b> (aluminum oxide, calcium phosphates including hydroxyapatite, carbon)	Very biocompatible, inert, strong in compression	Brittle, not resilient, difficult to make	Dental, femoral head of hip replacement, coating of dental and orthopedic implants
<b><i>Composites</i></b> (carbon-carbon, wire or fiber reinforced bone cement)	Strong, tailor-made	Difficult to make	Joint implants, heart valves

**2.2.2 Non-degradable/Permanent Orthopedic Implants.** Permanent implants have been traditionally and commonly used to secure serious fractures which usually need more structural and mechanical support.

**2.2.2.1 Metals.** Metals are often used as biomaterials due to their excellent electrical and thermal conductivity and mechanical properties. Commonly used metallic biomaterials include

stainless steels (SS), titanium (Ti) and cobalt-chromium (Co-Cr) based alloys. Metallic biomaterials are generally unreactive or neutral when implanted in bone, however they may cause a metabolically, bacteriologically, immunologically, or carcinogenic toxic release of ions/particles with wear and/or corrosion, leading to tissue loss/death (Jacobs, Hallab, Skipor, & Urban, 2003). Their neutrality, high mechanical strength, fracture toughness and corrosive resistance make metals well suited for load-bearing applications. Therefore, they are used as permanent, passive, hard tissue replacements in total hip and knee joints; for fracture healing aids as bone plates, screws and pins; spinal fixation devices; and dental implants (Park & Bronzino, 2002). However the elastic moduli of metals are most times too high compared to that of natural bone tissue, resulting in stress shielding effects that can lead to reduced stimulation of new bone growth and remodeling which decreases implant stability and causes loosening (Staiger, Pietak, Huadmai, & Dias, 2006). These stress shielding effects lead to a second surgery for implant removal after the bone has healed, especially in pediatric and adolescent patients (Castellani et al., 2011). Revision surgeries increase the cost of healthcare, and the health risks and recovery time for the patient (Staiger et al., 2006). The threads of metallic interference screws can cut into soft tissue grafts (Feldman, 2005). Wear and corrosion are also a concern because they may result in the disintegration of the implant material which will weaken the implant and expose the surrounding tissues and organs to harmful corrosion products (Park & Bronzino, 2002).

Metallic orthopedic devices such as screws, distort CT and MR imaging because of their ferromagnetic properties. Both titanium alloy and stainless steel devices can be imaged with CT, however the resolution when imaging Ti is better and there is less signal interference (Christensen, Dalstra, Sejling, Overgaard, & Bunger, 2000; Feldman, 2005).

**2.2.2.2 Ceramics.** Ceramic materials are polycrystalline compounds of metallic and inorganic non-metallic elements. They are hard, brittle materials that are highly wear resistant and have high compressive strengths and low ductility. Bioceramics should be biocompatible first and foremost, but also non-toxic, non-inflammatory and or non-carcinogenic. Bioceramics are relatively inert to body fluids and are commonly used in dental crowns. Inactive and Bioactive cements are often used to bind implants with bone and ceramic coatings are used to protect substrate materials or alter surface properties of other materials, such as highly corrosive metals in metal prostheses (Black & Kohser, 2007; Park & Bronzino, 2002).

**2.2.2.3 Composites.** A composite material is a non-uniform solid consisting of two or more different materials that are mechanically or metallurgically bonded together but maintain their individual characteristic structure and properties. Composites usually have recognizable interfaces between the materials and exhibit characteristic or combined properties which are not possible with the individual components by themselves. Composites are attractive biomaterials because they allow control over the material properties and can be stronger than steel, lighter than aluminum, and stiffer than titanium and have good fatigue life, low corrosion rates, and adequate wear resistance. Composites are used to reinforce other biomaterials and are used in dental and orthopedic applications such as implants with porous surfaces (Black & Kohser, 2007; Park & Bronzino, 2002).

**2.2.3 Biodegradable Orthopedic Implants.** These materials completely dissolve in the body over time.

**2.2.3.1 Ceramics.** Resorbable ceramic materials degrade at materialy-dependent rates when implanted. Many biodegradable implants and implant coatings are made of calcium

phosphate. Hydroxyapatite (HA) and tricalcium phosphate are often used for repairing or replacing bone tissue (Al-Sanabani et al., 2013; Black & Kohser, 2007; Park & Bronzino, 2002).

**2.2.3.2 Polymers/Plastics.** Plastics are lightweight, low-density materials that are very corrosive resistant and easy to fabricate. However they lack the mechanical strength compared to metals. Biomedical polymers, whether natural or synthetic, are expected to be biocompatible and sterilizable. Polyethylenes are the most common polymer but polylactic acid (PLA), poly-L-lactic acid (PLLA), and polyglycolic acid (PGA) are the most commonly used for interference screws due to their approval by the Food and Drug Administration (Eglin & Alini, 2008). Ultra-high-molecular-weight polyethylene (UHMW) is a commonly used orthopedic biomaterial in the acetabular cup hip replacements and the tibial plateau of knee replacements. Polymethyl methacrylate (PMMA) is a typically transparent material, with excellent optical and color properties that make it useful for dental applications as well as commonly used in orthopedic interference screws and bone cements. Another application of these materials include controlled drug release (Black & Kohser, 2007; Park & Bronzino, 2002). Polymers have good biomaterial attributes but polymer interference screws degrade at unpredictable rates, and must be monitored for chemicals degrading throughout the body, to avoid adverse effects (Eglin & Alini, 2008). Degradable polymers are not visible through radiography.

**2.2.3.3 Magnesium and its alloys.** Magnesium (Mg) is the fourth major cation of the human body, with 50% of the total amounts of Mg in the body in bone tissue. Magnesium is essential physiological functions of the cells including ion transport, energy metabolism and cell proliferation (Okuma, 2001). Magnesium is osteoconductive or stimulates bone growth (Castellani et al., 2011; Erdmann et al., 2011; Kim et al., 2014; Frank Witte et al., 2006; F. Witte et al., 2005; F. Witte, Ulrich, Palm, & Willbold, 2007; Zhang, Xu, Yu, Pan, & Yang, 2009).

Solid magnesium is the lightest commercially used metal that has a density of  $1.74 \text{ g/cm}^3$  and is 1.6 and 4.5 times less dense than aluminum and steel, respectively (Black & Kohser, 2007). Mechanically, magnesium is advantageous because its fracture toughness is greater than ceramic biomaterials such as hydroxyapatite, while its elastic modulus (between  $\frac{1}{4}$  and  $\frac{1}{5}$  that of steel) and compressive yield strength are closer to those of natural bone than is the case for other commonly used metallic implants (Table 2). Magnesium in its natural form has a low corrosion resistance, especially in electrolytic, aqueous environments like the human body (Kim et al., 2014; Frank Witte et al., 2006; F. Witte et al., 2005), losing mechanical integrity before bone has sufficiently healed and producing magnesium ions ( $\text{Mg}^{2+}$ ), hydroxide ions ( $\text{OH}^-$ ), magnesium hydroxide ( $\text{Mg}(\text{OH})_2$ ), and hydrogen gas ( $\text{H}_2$ ) (Kim et al., 2014). Magnesium's degradation products include a non-toxic hydroxide which is excreted in urine (Almarza, Holmes, Chung, & Henderson, 2014). Alloying elements and surface modifications such as protective coatings have been shown to slow magnesium's corrosion and change its degradation profile (Henderson et al., 2014; Kim et al., 2014). Common alloying metals are aluminum and zinc but so far alloying with rare metals have had the most significant effect on corrosion rate (F. Witte et al., 2005). Unlike traditional metallic biomaterials, magnesium creates minimal interference and is visible by MRI and CT without artifacts (F. Witte, Crostack, J., & Beckmann, 2001).

Table 2

*Summary of the physical and mechanical properties of various implant materials in comparison to natural bone (Staiger et al., 2006)*

<b>Properties</b>	<b>Natural bone</b>	<b>Magnesium</b>	<b>Ti alloy</b>	<b>Co-Cr alloy</b>	<b>SS</b>	<b>Synthetic HA</b>
-------------------	-------------------------	------------------	-----------------	------------------------	-----------	-------------------------

Table 2

*Cont.*

<b>Density</b> (g/cm <sup>3</sup> )	1.8-2.1	1.74-2.0	4.4-4.5	8.3-9.2	7.9-8.1	3.1
<b>Elastic modulus</b> (GPa)	3-20	41-45	110-117	230	189-205	73-117
<b>Compressive yield strength</b> (MPa)	130-180	65-100	758-1117	450-1000	170-310	600
<b>Fracture toughness</b> (MPam <sup>1/2</sup> )	3-6	15-40	55-115	N/A	50-200	0.7

### 2.3 In Vivo Performance of Orthopedic Biomaterials (Focused on Screws and Plates)

**2.3.1 Biological performance.** Bone's biological response to implants must be evaluated before and after implantation to prevent serious immunologic reactions. Over the years Witte et al. have investigated the biological performance of biodegradable magnesium implants. In 2005, they investigated the *in vivo* degradation of Mg-based alloys, comparing two alloys containing only aluminum and zinc (AZ31: 3 wt% aluminum and 1 wt% zinc, and AZ91: 9 wt% aluminum and 1 wt% zinc), and two alloys with rare earth element combinations (WE43: 4wt% yttrium and 3 wt% of a rare earth metal mixture consisting of neodymium, cerium and dysprosium, and LAE442: 4wt% lithium, 4 wt% aluminum and 2 wt% of a rare earth element mixture of cerium,

lanthanum, neodymium and praseodymium), along with a polylactide control. All the implants consisted of rods 1.5 mm in diameter and 20 mm in length, inserted into the femur of guinea pigs. Radiographs were taken frequently, and implants were harvested at 6 and 18 weeks. Synchrotron-radiation-based micro-CT was used to characterize the degradation of the implants, for which complete degradation was observed in 18 weeks. Subcutaneous gas pockets have been observed as soon as 1 week after implantation, which could be removed using a syringe, however adverse reaction had not occurred as is seen in many polymeric biomaterials. Energy dispersive X-ray analysis (EDX) showed that the rare earth elements were localized in the corrosion layer only and not in surrounding bone. X-ray diffraction (XRD) showed high levels of calcium and phosphorous that formed an amorphous calcium phosphate at the surface of the implanted material. Significantly increased bone area around Mg-based implants (F. Witte et al., 2005). Erdmann et al. used these methods, as well as scanning electron microscopy (SEM) to assess the *in vivo* degradation behavior of magnesium calcium alloy (MgCa0.8) by determination of the volume of metal alloy remaining and weight changes of retrieved screw samples (Erdmann et al., 2011).

Gaweda et al. (2007) clinically compared the results of bioabsorbable poly L-lactide interference screws (Arthrex, Naples, FL) and screw-posts (ChM, Lewickie, Poland) for hamstring graft distal fixation in ACL reconstructions in order to evaluate differences in outcome and bioabsorption of the devices. The authors compared results of ACL injury assessments on 14 patients' found that there is a lack of bioabsorption with poly L-lactide interference screws and that these screws frequently cause problems including minor to moderate pain (10 of 14 patients who had complications) intolerable pain and cyst formation (2 of 14 patients) and 1

patient had skin irritation, all leading to premature removal of the device (Gaweda, Walawski, Weglowski, & Krzyzanowski, 2009).

**2.3.2 Mechanical Performance.** For successful clinical employment, orthopedic implants must be able to withstand functional loading in host bone. Weiler et al performed a biomechanical poly-(D,L-lactide) interference screw study on sheep to evaluate the strength of interference screw fixation over time and to study the histological changes during the healing process. Pull-out tests after ACL reconstruction over 52 weeks determined that the graft fixation was not to be the weak link of the reconstruction, but the grafts, which failed at different places over the duration of study (Andreas Weiler et al., 2002). Gaweda et al. (2007) found that bioabsorbable poly L-lactide interference screws caused traumatic ACL graft ruptures related to twisting injury.

Castellani et al. investigated whether implant interface strength and osseointegration of a novel biodegradable magnesium alloy (chemical composition: Mg–Y–Nd–HfRE) was comparable to a titanium alloy control (Ti-6Al-7Nb). Implants 1.6 mm in diameter and 7 mm in length were implanted into the femurs of rats. The Mg-alloy had the higher maximum push-out force, ultimate shear strength and energy absorption to failure after implantation times of 4, 12 and 24 weeks. Micro-CT showed much higher bone-implant contact and bone volume per tissue volume for the Mg implants than Ti alloy implants. They found the Mg implant had enhanced bone response, better osseointegrative properties and implant-interface strength and no inflammatory reactions in the animals (Castellani et al., 2011).

Erdmann et al. (2011) performed uniaxial pull-out tests on degradable magnesium calcium alloy (MgCa0.8) screws and commonly used stainless steel (S316L) screws at a rate of  $0.1 \text{ mms}^{-1}$ . They found no significant differences between the pull-out forces of MgCa0.8 and

S316L, two weeks after surgery ( $P = 0.121$ ). However, six weeks after surgery the pull-out force of MgCa0.8 decreased slightly. In contrast, the S316L pull-out force increased with time since significantly higher pull-out values were detected for S316L from 4 weeks on ( $P < 0.001$ ). The volume and weight of MgCa0.8 gradually reduced and a corrosion layer (mainly composed of oxygen, magnesium, calcium and phosphorus) formed on the implants.

## **2.4 Mechanical Testing of Biomaterials and Orthopedic Devices**

**2.4.1 Introduction.** The mechanical properties of orthopedic devices such as stress, strain and energy and the elastic modulus, shear modulus and Poisson's ratio of biomaterials cannot be measured directly. Indirect measurements such as force (based on reactive forces) or electrical resistance are taken and the desired characteristics are determined mathematically.

**2.4.2 Destructive and proof testing.** Destructive testing allows machined orthopedic devices to be characterized mechanically and tested for material flaws by subjecting the device to conditions that induce failure. This gives insight into the device's performance under those conditions. In proof testing, the materials are subjected to a load or pressure that equals or exceeds the design's limit. If the device holds up under these conditions, then it is accepted that the device will perform at the expected level. However this form of testing is expensive because of equipment costs and the fact that the samples are destroyed during the test. (Black & Kohser, 2007).

**2.4.2.1 Universal testing machines (UTMs).** UTMs are usually used to destructively test samples at a known loading rate until maximum stress/load occurs. This test gives a stress-strain curve as well as the stress under maximum load and the elastic modulus of the material. Common tests performed with these machines are stiffness, torsion and pull-out tests for screws (Christensen et al., 2000). Testing procedures of UTMs are standardized by ASTM or the ISO

and are specific to the type of test. For example, testing axial pull-out strength as prescribed in ASTM F-543) or testing femoral implants as prescribed in ISO 7206-4, 7206-6, and 7206-8. The mechanical properties of bone implant screws are tested by torsional fracture testing, which applies torque at a constant rotational speed until the screw fails; screw-in testing by screwing bone screws at constant force and constant speed into simulated bone to evaluate the screw-in properties; and pull-out testing, which pulls screws out of synthetic bone (ASTM F-1839) at a constant rate to evaluate the fixation of the bone screws (Chapman et al., 1996; Zdero, Elfallah, Olsen, & Schemitsch, 2009). These tests are commonly used to perform physical validation of finite element analyses. Bone plates are usually tested by bending tests (Corporation, 2013).

**2.4.3 Non-destructive testing.** Non-destructive testing the device is preserved and can be used again. The same sample can be used for repeated tests without issue for cost (after initial equipment costs) or number of available samples. However results are usually qualitative or comparative and require a specialist for interpretation. Periodic non-destructive testing can guide the design process and the performance over time after production (Black & Kohser, 2007).

#### **2.4.4 Testing Methods**

**2.4.4.1 Nanoindentation and Atomic Force Microscopy (AFM).** Atomic force microscopy and nanoindentation is used to observe the properties at the surface of materials. AFM works by an indentation cantilever indenting a surface and plotting or “imaging” the indentation. Sharper indentation tips give better results. AFM is able to characterize the surfaces of metallic implants or their coatings by measuring forces at the nano-scale level using a tapping mode, which uses less force and is suitable for softer materials. Scratching or wear tests are used for determining the adhesion of surface films and coatings (Salahinejad et al., 2013;

Schmitt, Elings, & Serry, 2010; Wu et al., 2008). Nanoindentation works well for small heterogeneous surfaces, but may introduce errors in the computed mechanical properties when indenting near the interface between two materials having significantly different mechanical properties (Leong & Morgan, 2008; Zhao & Ovaert, 2010). Nanoindentation is used for measuring the mechanical properties of new/woven bone.

## **2.5 Introduction to Finite Element Analysis**

**2.5.1 Introduction.** The finite element (FE) method is often used in structural mechanics applications, including biomechanics, because of its ability to accurately solve differential equations over complex geometries, like orthopedic implants, or which have distributions of material properties, like bone. The method of finite element analysis (FEA) is commonly used to evaluate the mechanical behavior of bone tissue and of load-bearing implants such as screws and plates (Klues, 2010). By dividing an object into model building blocks called elements, defined by reference points called nodes (Figure 2), the behavior of an object in response to external loads can be estimated by the deformation of the elements. Boundary conditions and material properties must be applied to each element for these deformations to be recorded. FEA becomes more accurate when the object is divided into more elements, however it also becomes more computationally expensive (Klues, 2010). The stresses, strains, strength and stiffness of bone can be estimated or predicted. FEA expedites the implant design process by evaluating candidate designs before prototypes are created for clinical or radiographic trials begin and eliminating unsuitable designs, thus reducing the cost of testing and time to market (Bartel et al., 2006; Klues, 2010). With FEA, local stress and strains of the bone and stress-shielding effects of the device can be investigated. If the device is much stiffer than the bone, as is the case with

many traditional metal implants, bone may be loaded insufficiently causing bone resorption around implant and subsequent implant failure (Bartel et al., 2006; Kluess, 2010).

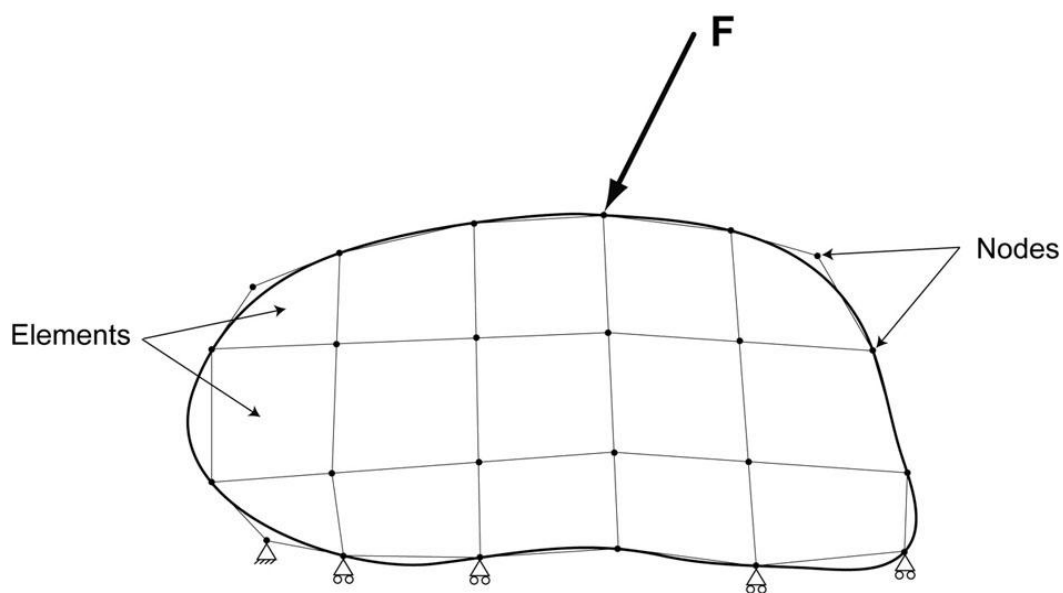


*Figure 2.* Diagram of a finite element model with a finite number of discretized elements and nodes, as well as boundary conditions (E. F. Morgan & Bouxsein, 2005).

## 2.6 CT to FEA for Orthopedic Applications

**2.6.1 Introduction.** The biomechanical interactions of bone tissue and implanted devices cannot be measured directly, but they can be estimated using micro-CT scanning to finite element analysis workflow. This method bridges the gap between clinical and engineering approaches to testing biomedical devices.

**2.6.2 General method for CT to FEA studies.** Computed Tomography of the desired biological tissue is performed. 3-D images from the CT allow for geometric models that are highly accurate in the external representation and just as defined internally. Image processing software is used to reconstruct data and create meshes, and material properties are mapped onto the mesh. These meshed parts must be compatible with finite element software. Boundary and load conditions are assigned to the model and the simulation is run (Herrera et al., 2012).

### **2.6.3 CT to FEA studies of bone.**

**2.6.3.1 *Ex vivo studies.*** Several subject specific CT to FE models have been used for human bone, especially the femur (Fulvia Taddei, Cristofolini, Martelli, Gill, & Viceconti, 2006; F. Taddei, Martelli, Reggiani, Cristofolini, & Viceconti, 2006; Viceconti, Davinelli, Taddei, & Cappello, 2004). High resolution magnetic resonance imaging (HR-MRI) and micro-computed tomography ( $\mu$ -CT) and quantitative computed tomography (QCT) allow geometrically and materially accurate finite element models of bone to be created (E. F. Morgan & Bouxsein, 2005). FE models can be created by the voxel or structural method. The voxel method involves directly converting each image voxel of bone into cubic/8-noded hexahedral elements (J. H. Keyak, Meagher, Skinner, & Mote Jr, 1990). The voxel method is advantageous because it is semi-automated but disadvantageous because of computational cost and time and the fact that the cube-shaped elements cause significant errors, especially at surfaces (van Rietbergen, Weinans, Huiskes, & Odgaard, 1995). Another method is to extract 3D surface geometry from QCT data, meshing this geometry, then mapping material properties from QCT density values (J. H. Keyak et al., 1990; Viceconti et al., 2004). This approach is more accurate and gives better surface stresses and strains than the voxel method (Fulvia Taddei et al., 2006; Viceconti et al., 2004). CT to FE has been researched and a semi-automated process has been developed. However those models work for bone only.

QCT-based FE studies have been done to compare FE and experimentally predicted bone strength/failure loads (Cody et al., 1999; Joyce H. Keyak, Rossi, Jones, & Skinner, 1997) and to predict location and type of fracture (J. H. Keyak, Rossi, Jones, Les, & Skinner, 2001) of the proximal femur. High resolution pQCT (HR-pQCT)-based FE studies have also been done to

assess load transfer characteristics and the biomechanical effects of osteoporosis (Pistoia et al., 2002; Ulrich, van Rietbergen, Laib, & Rügsegger, 1999) in the distal radius.

**2.6.3.2 *In vivo* studies.** *In vivo* studies are fewer than *ex vivo*, but QCT-based FEA has been done to study vertebral strength (Faulkner, Cann, & Hasegawa, 1991) and effects of glucocorticoid treatment on femoral strength (Lian et al., 2005) in postmenopausal women.

**2.6.4 CT to FEA of *in vivo* magnesium devices.** Current CT to FEA processes for *in vivo* implants models the implants and bone separately then combines them into a single model (Figure 3). Henderson et al. investigated commercially available magnesium alloy, AZ31, for use as a biodegradable craniofacial screw. Pure Mg and AZ31 screws were implanted in New Zealand White rabbit mandibles for 4, 8 and 12 weeks with controls of an osteotomy and a stainless steel screw implanted for 12 weeks. Qualitative micro-CT analysis of the pure Mg and AZ31 screws at 12 weeks showed craniofacial bone remodeling around both screw types. Mg alloy screws had different degradation rates depending on whether the implant was placed in cortical bone, marrow space, or in muscle. *In vitro* pull-out tests showed that pure Mg and AZ31 screws had a holding strength of about 40 N, similar to stainless steel screws. The *in vitro* pull-out tests were simulated by custom 3-D FE software, to determine how different mechanical properties affected the pull-out strength. The FE models showed that pull-out strength does not change much with constant screw diameter and interfacial conditions. The FEA also showed that the screw-bone interfacial strength greatly affects pull-out strength (Henderson et al., 2014).

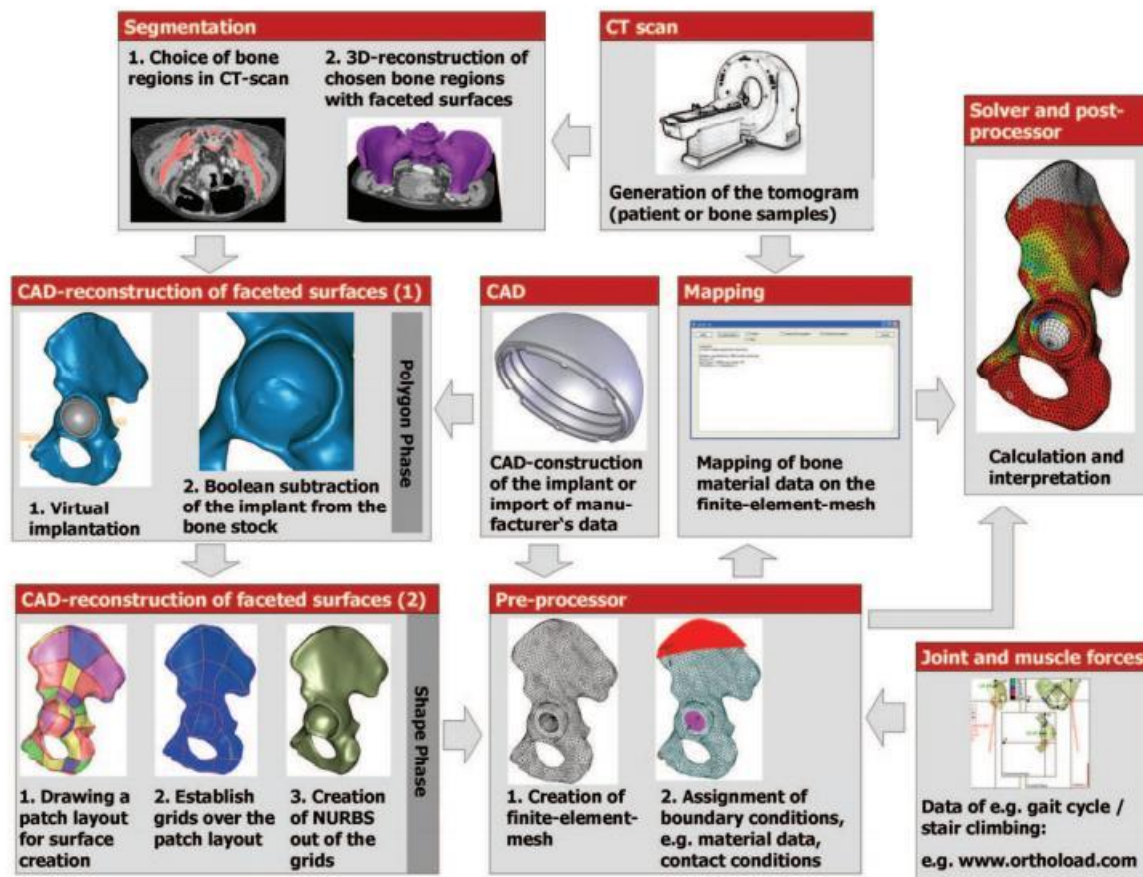


Figure 3. CT to FEA process of an implant-bone-compound (Kluess, 2010).

Very little CT to FEA research has been done on magnesium and its alloys *in vivo* and there is a significant gap in knowledge in this area.

Finite element analysis based on CT can be used to predict the biomechanical performance of Mg devices pre-clinically, saving money and time for developers of the devices and getting it closer to FDA approval and commercial success. This method is a preferable first step to clinical and experimental testing because design and device properties can be modified to evaluate the device before prototypes are even manufactured and boundary conditions such as natural musculoskeletal forces in the body can be tested. Computational models like those

proposed in this research are also easier to interpret and testing does not require significant material resources.

## CHAPTER 3

### Methodology

#### 3.1 Micro-Computed Tomography to Finite Element Analysis Study

**3.1.1 Samples.** Samples were previously acquired by personnel in the NSF Engineering Research Center for Revolutionizing Metallic Biomaterials (NSF ERC-RMB) for an NC A&T Institutional Animal Care and Use Committee-approved study investigating *in vivo* degradation of an unnamed magnesium (Mg) alloy. Magnesium-alloy (test) and 82:18 PLLA:PLGA copolymer (control) orthopedic screws of 3 mm in diameter and 5 mm in length were press-fitted into 3 mm osteomies transcortically in the right and contralaterally in the left femoral condyles of 12 six month old female New Zealand White rabbits, respectively. Titanium (Ti) K-wires were placed proximal and distal to the implants as a marker, in the event that the implants fully degraded. The animals were euthanized at 2, 4, 12, 24, 36 and 52 weeks after implantation to extract the condyles with devices and Ti K-wires in place.

**3.1.2 Micro-CT scan acquisition.** The Nanotom-M<sup>TM</sup> Computed Tomography System (GE Phoenix Nanotom-M 180, GE sensing & Inspection Technologies GmbH, Germany) (Figure 4), used for Revolutionizing Metallic Biomaterials Research, Education, and Training was previously acquired through the National Science Foundation Award # 0959511. NSF ERC-RMB personnel previously used high resolution x-ray computed tomography to scan explanted condyles containing the implants and K-wires at each of the 6 time points. Throughout the experiment, the parameters used for the  $\mu$ -CT scanning varied due to revisions over the period of the study caused by technical issues, software upgrades and the learning curve of the researchers, as it was the first long-term explants study in the ERC. The x-ray tube had a tungsten target, which was typically operated at 80 kV and 80  $\mu$ A. Whole condyle scans were acquired by the

mounted sample being revolved  $360^\circ$  to give 1000-1500 projections per sample, with an average 2-3 scans per position. The mount revolved by  $0.36^\circ$  and  $0.24^\circ$  with each of 1000 and 1500 projections per sample respectively, based on the following equations:

$$\text{With 1000 projections, } \Delta\theta = \frac{360^\circ}{1000} = 0.36^\circ$$

$$\text{With 1500 projections, } \Delta\theta = \frac{360^\circ}{1500} = 0.24^\circ$$

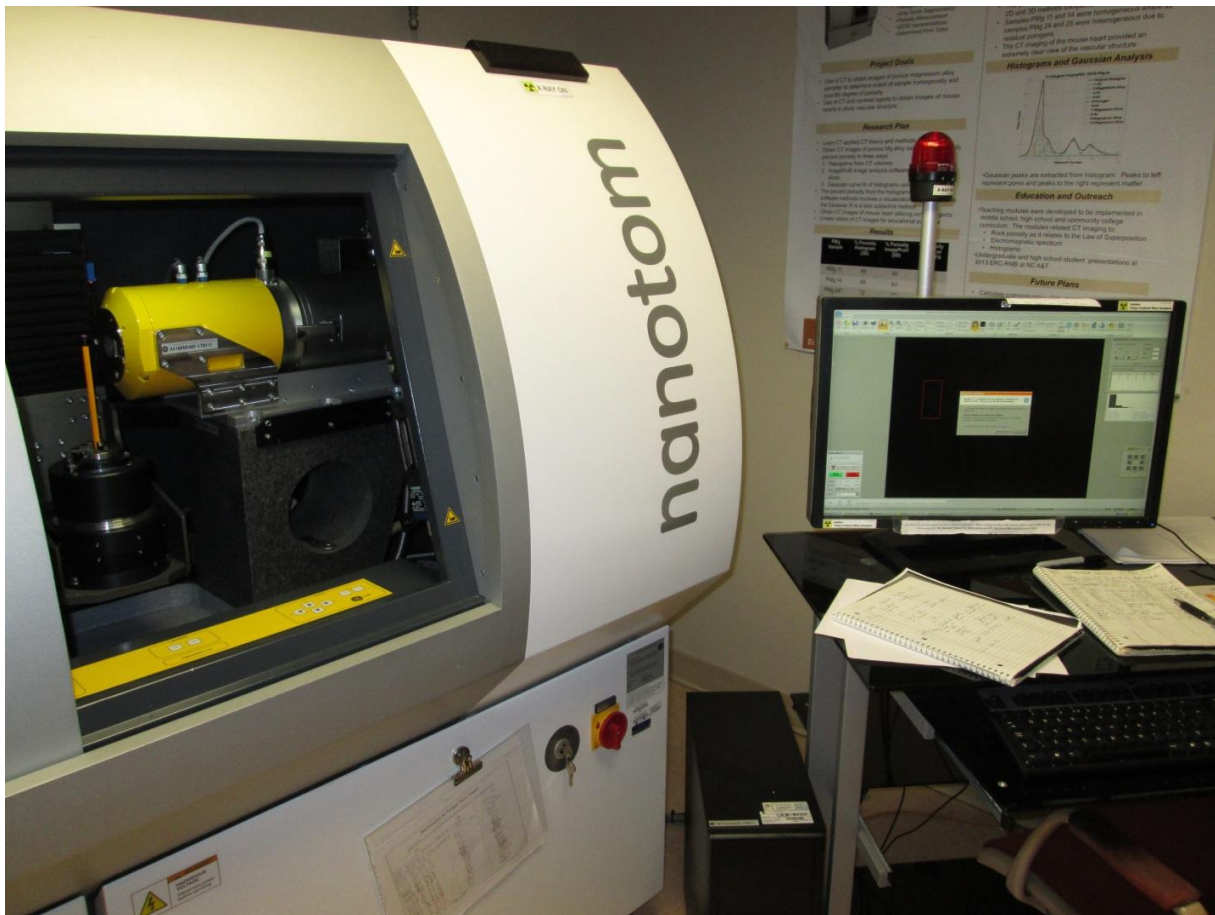


Figure 4. The Nanotom M micro-CT machine setup, with mounted 2B pencil.

**3.1.3 Micro-CT reconstruction and data processing.** The micro-CT scan data for the right condyles at each time point were reconstructed with the in-house reconstruction software from GE. Reconstructed data were processed through VG Studio Max 2.1 software (Volume

Graphics GmbH, Germany) and exported as 2-dimensional DICOM (.dcm) image stacks of the scan. These DICOM files were exported to an external disk in the orientation with the least amount of slices, in order to save disk memory. At the time of export, the image width and height, pixel size and distance between slices were noted (Table 3).

Table 3

*Information on the DICOM image stacks from micro-CT scans.*

Image information	Week of explantation		
	4	24	52
No. Of Slices: X	1140	1033	1142
No. Of Slices: Y	2171	2331	2211
No. Of Slices: Z	1041	1032	950
Pixel size (mm)	0.01	0.011	0.01
Slice distance (mm)	0.0193	0.02	0.0182

**3.1.4 3-D Volume segmentation.** The DICOM image stacks were manually imported into Mimics (Materialise, Leuven, Belgium), using the image information collected in the previous step. The orientation of the image was selected by selecting top and bottom, anterior and posterior and right and left of the image stack. The regions of the imported scans were segmented in 2-D by thresholding into “masks” of visually selected ranges of Hounsfield Unit (HU) values from 0 to 64,511. Hounsfield Units represent the attenuation of x-rays by an object’s features, based on the standards such as air, which has a HU value of -1,000 and water which has a HU value of 0.

At each time point, masks were created for the undegraded core of the screw and the surrounding degraded/corrosion product, for the titanium (Ti) K-wires which were implanted proximal and distal to the device, and the host bone (Table 4). Noise was removed noise from the entire model. The Ti mask was created with HUs from 32,000 to 64,511. The undegraded/integrous portion of the screw or the screw core mask was created with HUs from 9,000 to 13,500. These ranges also included non-screw pixels especially around bone, which had to be removed using the volume edit function. To create the corrosion product mask, HUs 6,000 to 11,000 were selected. However outlying pixels were present in the bone and screw core. To fix this, the core mask was subtracted from corrosion product and the other pixels in bone were removed using the volume edit function. Finally, the bone mask was created by selecting HUs 226 to 64511 in a mask for preliminary use, then subtracting the corrosion product, Ti wires and screw core masks from the preliminary one. The Ti K-wire, screw core and bone only masks (Figure 5). The “Calculate 3D” function was used on each of the masks to render the 3-D version of the mask.

Table 4

*Masks of the scan components created in Mimics by thresholding*

<b>Mask</b>	<b>Color</b>	<b>Min. HU Value</b>	<b>Max. HU Value</b>
<b>Ti K-wires</b>	Yellow	32000	64511
<b>Corrosion product</b>	Cyan	6000	11000
<b>Screw core</b>	Red	9000	13500
<b>Bone only</b>	Blue	226	64511

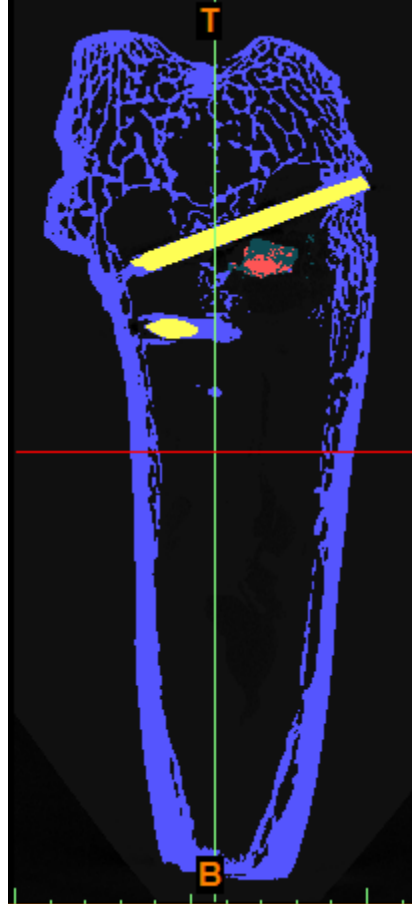


*Figure 5.* Segmented masks in of the  $\mu$ -CT data in Mimics.

**3.1.5 Material property assignment.** Material properties were assigned to the masks (Figure 6) based on the distribution of the HUs or assigned a single material property across the entire volume from literature. Single values from literature were used for the parts of the samples that were homogenous and had published values, such as the Ti wires.

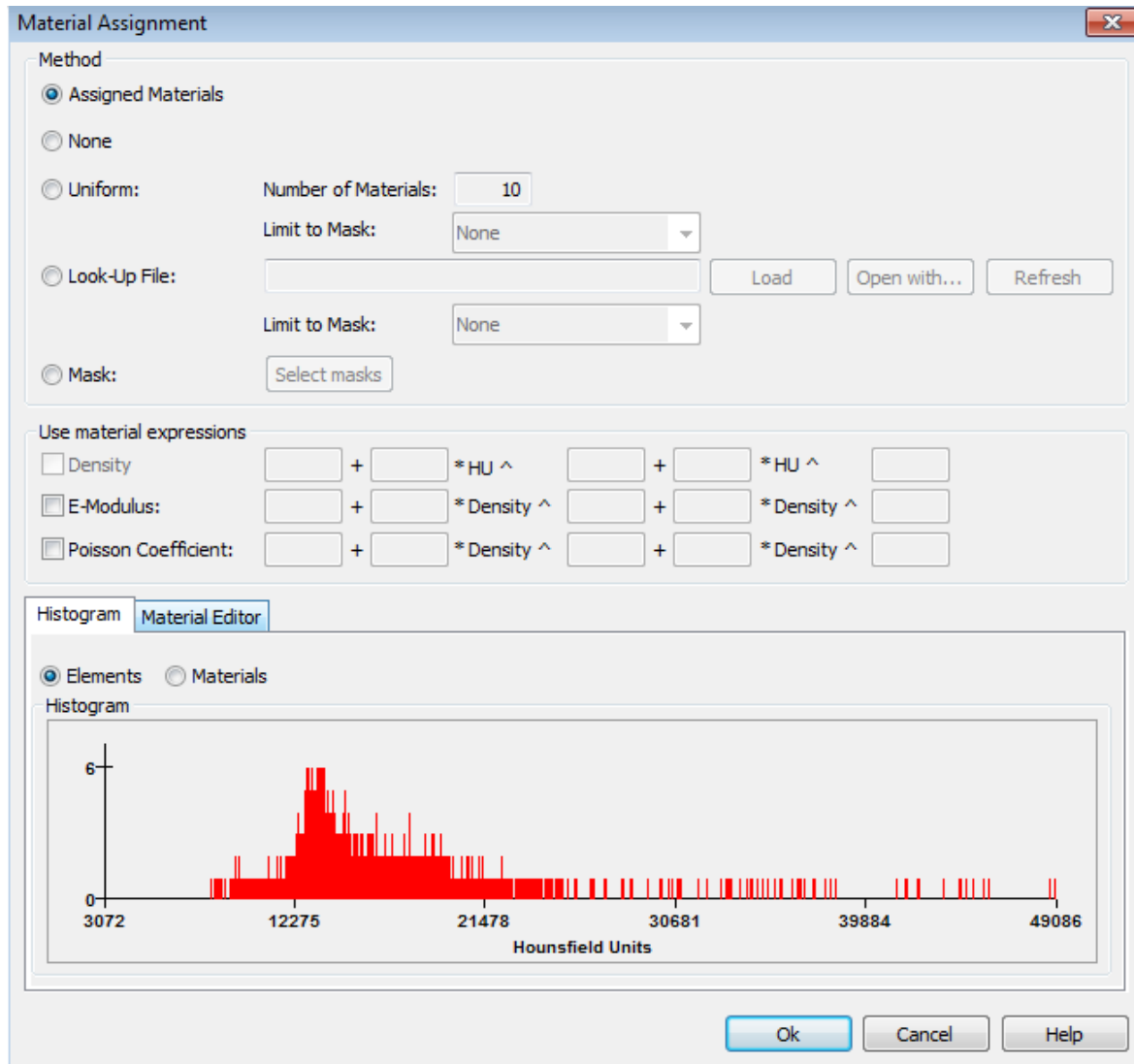


Figure 6. Material property assignment tab in Mimics with histogram of Hounsfield units in a model.

### 3.1.6 Meshing

**3.1.6.1 Mimics.** Mimics was used to generate a linear tetrahedral (4-node) and a linear hexahedral (8-node) volume mesh of each mask. The quality or resolution of the mesh was controlled by changing the voxel grouping or XY and Z resolutions iteratively. The best resolution that the computer and program could process was sought. The numbers of elements

produced for each mask were recorded. The volume mesh generated by Mimics was exported in the Abaqus (.inp) file format.

**3.1.6.2 3-matic.** 3-Matic (Materialise, Leuven, Belgium) is an add-on finite element tool for Mimics. 3-Matic was also used to create a volume mesh of the masks using the “remesh” function. The “autofix” function was used to correct any bad triangles in the mesh before remeshing to control mesh quality and obtain the lowest possible element number. The element type was changed to and from linear (4-node) and quadratic (10-node) tetrahedral elements in order to save meshes with both element types. The meshed masks were exported in the Abaqus (.inp) file format.

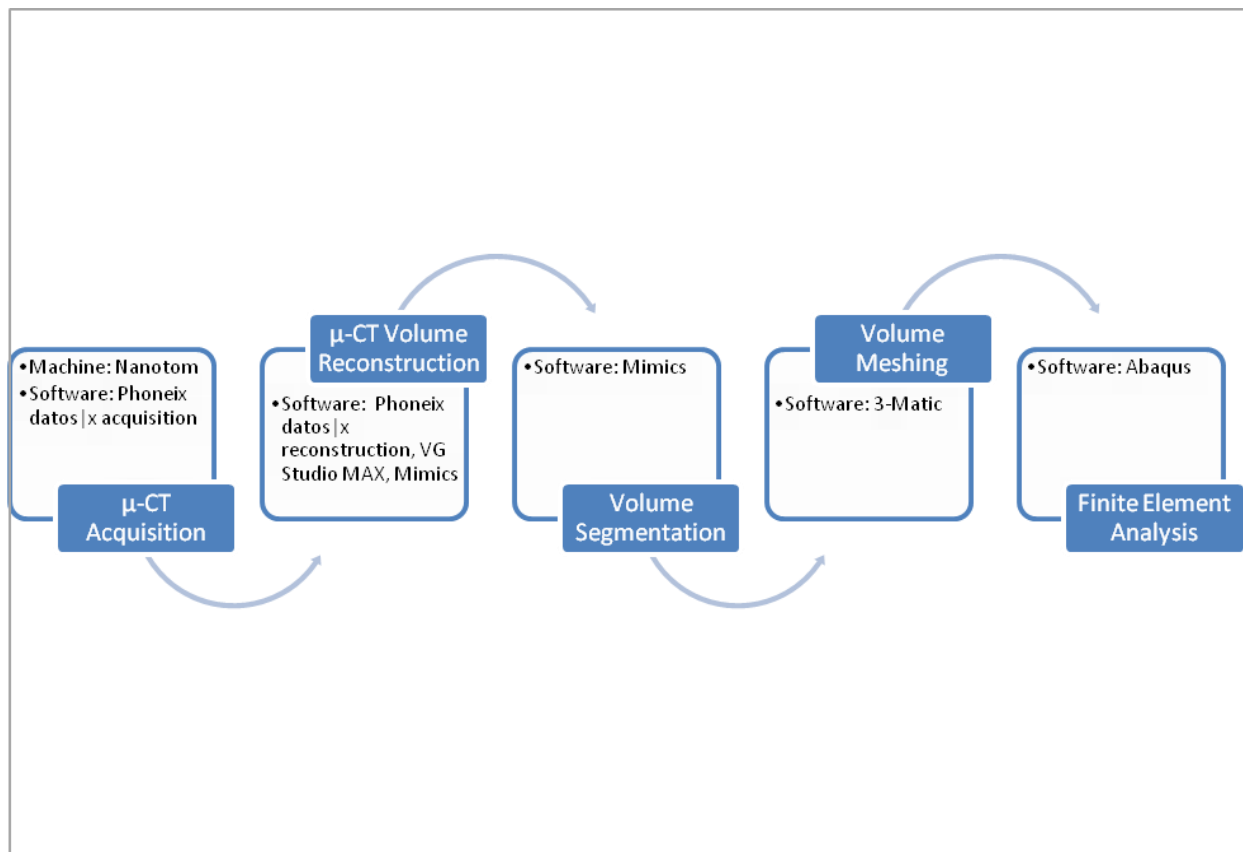


Figure 7. Flow chart of μ-CT to FEA protocol used.

**3.1.7 Finite Element Analysis (FEA).** The meshed masks (.inp) were imported into Abaqus as separate models. The material properties were adjusted from multiple (from HUs in Mimics) to single (assigned average in Abaqus), for parts as needed, for simplicity of the models. An assembly of the models of the different masks was created by creating instances of each mask to be combined into a single model of the degrading screw in bone as they appeared in the CT data. The models should align because they were all created from the same scan, with the same coordinate system. Boundary conditions including fixing the bottom of the model in the three translational degrees of freedom and a 0.3 mm axial displacement (to simulate pullout) were applied to the model for a quasi-static analysis.

### **3.2 FEA of Screw in Woven Bone**

This model was created for investigation of the Mg-based and the copolymer screws in woven bone, to generate foundational information about the mechanical behavior of these devices in woven bone and of the bone in response to the devices.

**3.2.1 3D CAD Model.** The 3D Computer Aided Design (CAD) model of an original baseline Generation One Johnson and Johnson screw with dimensions of approximately 5.2 mm in diameter and 15 mm in length with a full cannulation, a 2 mm pitch, a flattened head and no taper (Hawkins, 2013) (Figure 7) was imported to SolidWorks (Dassault Systèmes SolidWorks Corp.; Waltham, Massachusetts, USA). A 20 mm diameter by 20 mm length cylinder with the screw geometry removed from its center from top surface of the screw head (Hawkins, 2013), was also imported to SolidWorks. An assembly was created by placing the screw into the cavity in the bone block. This way, the screw was fully embedded in and surrounded by bone, as is the assumption of the press-fit implantation procedure described in the animal study above. The assembly was saved so that the parts would be recognized individually by the finite element

software, though fitted together. The assembly was saved in an IGES (.igs) format, which can be read by most finite element software.

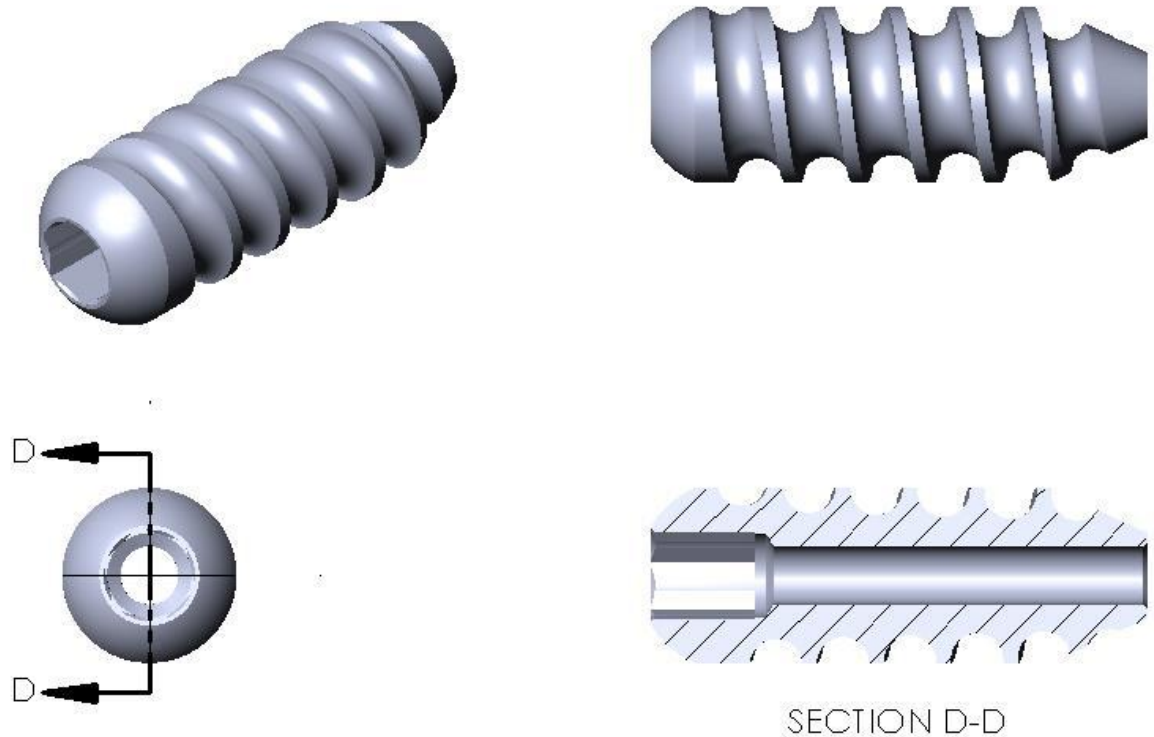


*Figure 8.* CAD drawing of the original baseline Generation One Johnson and Johnson screw design (Hawkins, 2013).

**3.2.2 Material Properties.** All materials in the models were assumed to be linear elastic and isotropic as in previous research (Chatzistergos, Magnissalis, & Kourkoulis, 2010; Hou, Hsu, Wang, Chao, & Lin, 2004). For the models involving the Mg-alloy, the screw region was assigned an elastic modulus of 45 GPa and a Poisson's ratio of 0.35. For the models involving the copolymer, the screw region was assigned an elastic modulus of 7 GPa and a Poisson's ratio of 0.36 (Jamshidian, Tehrany, Imran, Jacquot, & Desobry, 2010; Pietrzak, Caminear, & Perns, 2002). Values for the maximum and minimum nanoindentation moduli of woven bone (Leong & Morgan, 2008) were assigned to the bone as elastic moduli in MPa. A list of the materials and their properties are given in Table 5.

Table 5

*Material properties assigned to the bone, Mg-alloy screw and PLLA:PLGA screw in the FE models*

Material Properties	Material			
	Woven bone (min)	Woven bone (max)	Mg-alloy	PLLA:PLGA copolymer
Density (g/cm <sup>3</sup> )	0.62	0.62	1.74	1.24
Poisson's Ratio	0.3	0.3	0.35	0.36
Elastic Modulus, E (Pa)	26.9E+06	1010E+06	45.0E+09	7.00E+09

### 3.2.3 Finite Element Analysis

**3.2.3.1 Finite Element Software.** All aspects of the finite element analysis (FEA) were performed in Abaqus version 6.13 (Dassault Systèmes; Waltham, Massachusetts, USA). The IGES file of the screw and bone were imported as an assembly but identified as individual regions for the purposes of material property, mesh and load assignments.

**3.2.3.2 Meshing and convergence.** The screw-bone assembly was seeded with a global seed size of 0.0015. The assembly was meshed as a single part using quadratic (higher order) tetrahedral elements, denoted C3D10 in Abaqus. A surface mesh of the part is first laid, which is expanded into the volume mesh. As this screw in block design was previously tested by Hawkins (Hawkins, 2013), no convergence testing was needed for this study. Following from Hawkins, the number of elements used was over 23,355 (Figure 8).

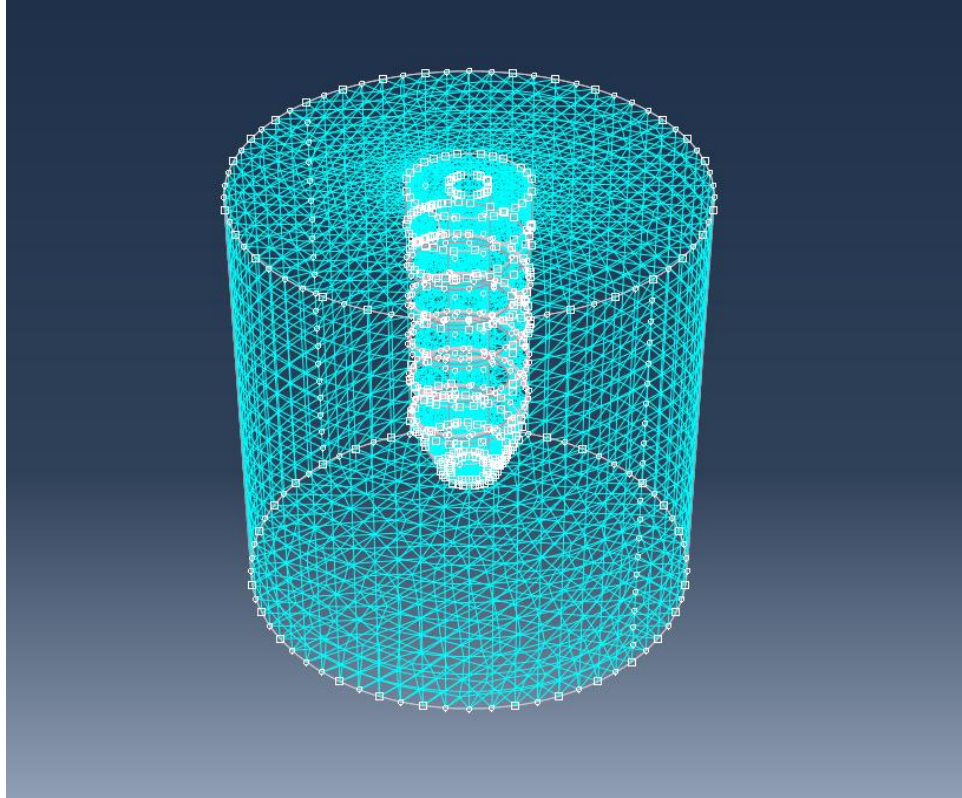


*Figure 9.* A wire-frame rendered model of the mesh and nodes of the model.

**3.2.3.3 Model Validation.** Like convergence, validation was conducted by Hawkins to test the reliability of the results obtained by the finite element analysis using the baseline screw model and a failure force equation (Chapman et al., 1996; Hawkins, 2013). The basis of the test is that the predicted shear failure force of 254.39 N (Hawkins, 2013), resulting from the equation directly relates to the experimental reaction or pullout force of the model.

### **3.2.4 Simulation**

**3.2.4.1 Models.** Once the IGES file was imported to create the first model, it was copied into three new models for a total of four models in all to test both the Mg-alloy and copolymer screw in woven bone with minimum and maximum elastic moduli,  $E_{\min}$  and  $E_{\max}$  respectively. The models generated were: Mg-alloy in  $E_{\min}$  woven bone, Mg-alloy in  $E_{\max}$  woven bone, 82:18 PLLA:PLGA in  $E_{\min}$  woven bone and 82:18 PLLA:PLGA in  $E_{\max}$  woven bone.

**3.2.4.2 Boundary conditions.** In the initial step, the bottom surface of the bone was fixed in all translational degrees of freedom. This was found by Hawkins (Hawkins, 2013) to give force values most similar to those predicted by an equation that predicts screw purchase (Chapman et al., 1996). Whereas in the second step an axial displacement load was applied to the screw head in the vertical direction to simulate a pullout test (Figure 9). The models were fixed by the bottom surface of the bone block to allow investigation of the effects of pullout on the bone-screw interface. A displacement of 0.3 mm was used because Hawkins, in his validation study, showed that the screw threads in this model failed at this displacement (Hawkins, 2013).

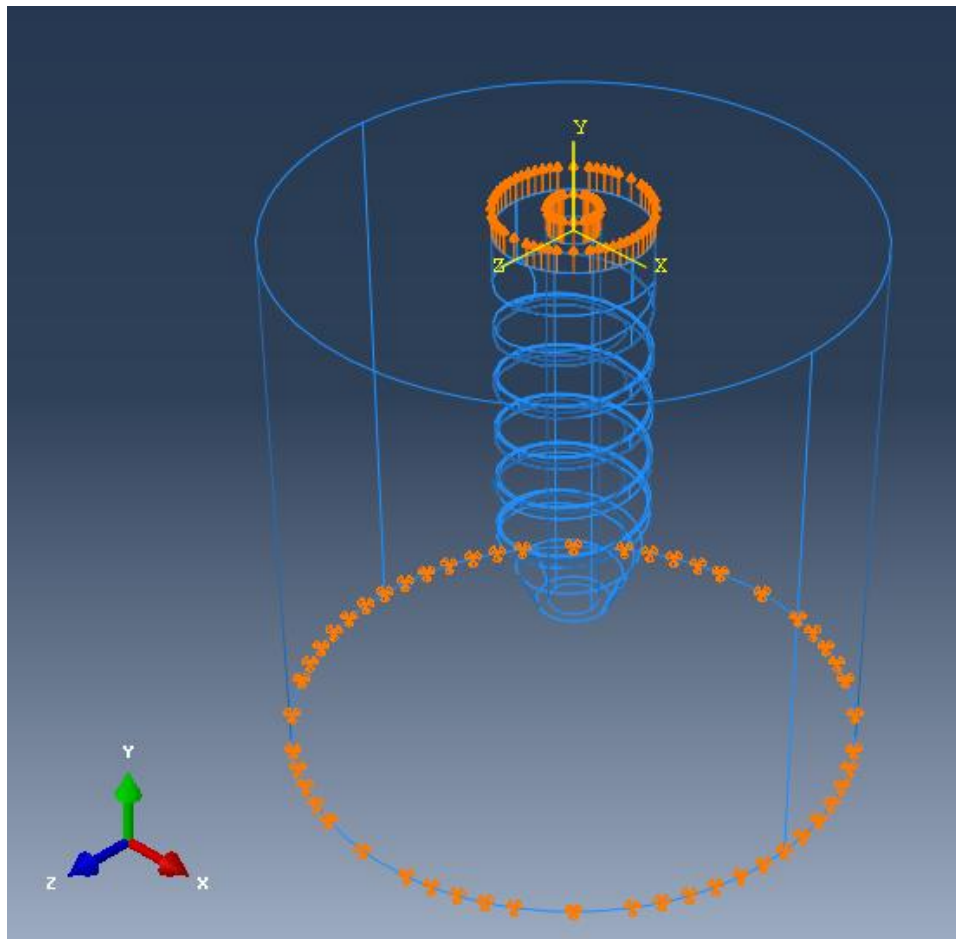


*Figure 10.* Boundary conditions used in the finite element models.

**3.2.5 Analysis.** A quasi-static (independent of time and inertia) analysis was run on the four models were run to determine the mechanical effects of Mg-alloy and copolymer screws in bone. The maximum reaction force (RF) results and translation (UT) were extracted from the results and used to determine the pullout force on the screw that will cause failure in the bone. Contour plots of the reaction force and translation results were created.

## CHAPTER 4

### Results

#### 4.1 Micro-CT to Finite Element Analysis

**4.1.1 Meshing in Mimics and 3-Matic.** In Mimics, all reconstructed objects were automatically assigned a triangular surface mesh.

**4.1.1.1 Mimics.** Mimics was successfully used to create tetrahedral volume meshes of all the masks. The number of elements that Mimics tried to export for a single part was 1-2 billion. The computer was not able to create a mesh with that many elements. The program crashed. Changing the voxel grouping by adjusting the XY and Z resolution at the same increments between 1 to 128 allowed a mesh to be created (Figure 10), though it was much less refined. Each mask volume and mesh type had minimum XY and Z resolutions for which the program could create the mesh. Some of the meshes were very rough and the shape of the mask was not well preserved (Figure 11).

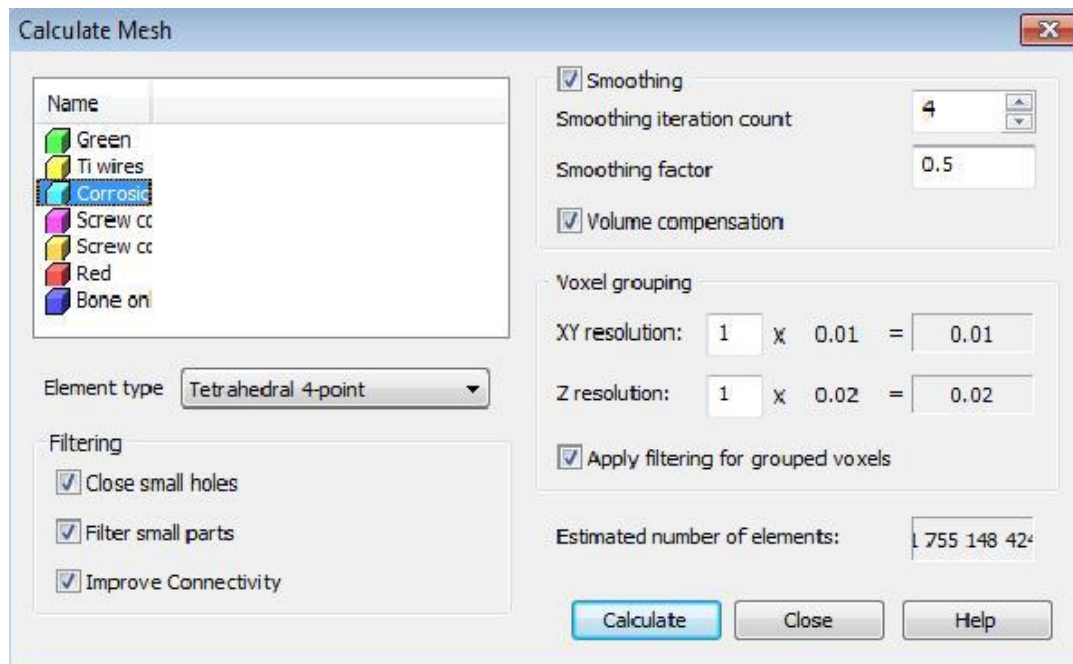


Figure 11. The volume meshing options in Mimics.

**4.1.1.2 Meshing in 3-Matic.** The remesh function in Mimics opens its add-on 3-Matic, where the operation is performed. Once in 3-Matic, the automesh function is used to automatically refine the existing surface mesh. The automesh function was successfully used to reduce the number of surface elements in the mesh up until a point that the element number remained unchanged. In general it took two or three runs of the automesh function to get to a point where the number of elements did not change. After the surface element number was reduced, the volume mesh was generated. Most of the masks had bad triangles (distorted, with flat or sharp angles) that were highlighted and fixed with a few uses of the autofix function. This combination of remeshing and fixing led to successful volume meshing of all the masks except the bone (Table 6). 3-Matic repeatedly failed to remesh the femur and resulted in the program crashing. A smooth wire frame of the masks/model could not be generated and exported to Abaqus for meshing.

Table 6

*Basic characteristics of the volume meshes of the in vivo device generated in 3-matic.*

<b>Mask</b>	<b>No. of volume elements</b>	<b>No. of nodes</b>
<b>Corrosion product</b>	12141	3778
<b>Ti wires</b>	5127	1600
<b>Screw core</b>	8655	2878

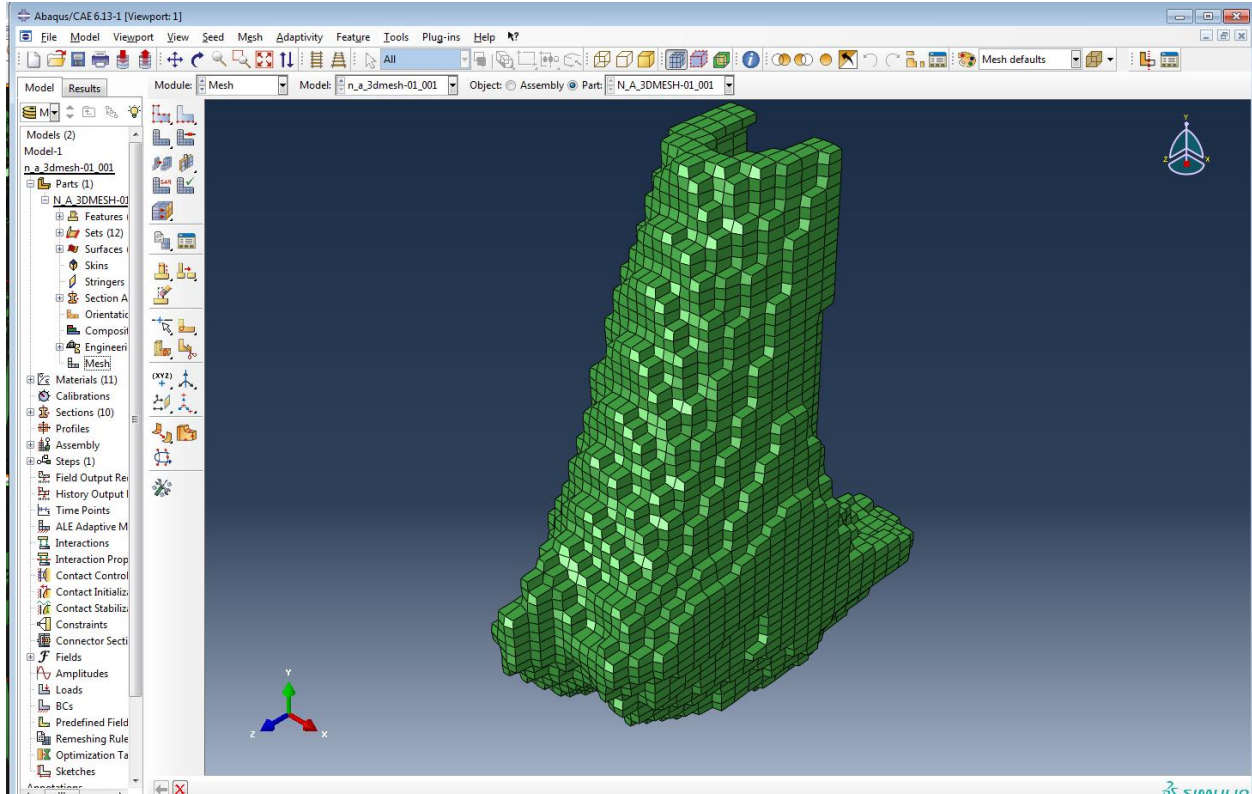


Figure 12. Hexahedral (8-node) mesh of about 36,000 elements created by Mimics but imported into Abaqus.

**4.1.2 Finite Element Analysis Job.** The geometry of the bone-screw construct was exported from Mimics in INP (Abaqus) file format. Though the model was successfully imported into Abaqus, the program did not recognize the geometry. The model was also exported in the STL format and opened in CAD program SolidWorks, where the model could be converted to INP format. However SolidWorks was not able to recognize the geometry either. The meshed masks from Mimics could not be sectioned into new sets or regions because Abaqus did not recognize the geometry. Each of the models had a set that had all the nodes and all the elements of that model. These elements or nodes could not be edited (changed to another shape or order) because element sets could not be selected on the models. Through the edit mesh feature, nodes and elements could only be deleted and then redrawn manually. The error

message received with attempts to change the mesh type was that there was a dependent orphan mesh.

When instances were created with an independent/parent part (assigned to bone) and the dependent/children parts (assigned to the Ti wires, and screw parts, to try to combine the models, the models still did not combine. Instead, only the bone was visible, even when the other models were selected.

A job was successfully created but aborted almost immediately after submission due to the following errors:

- “Normal cannot be computed in 1980 elements. The nodal coordinates may be incorrect or the element aspect ratio may exceed 1000 to 1.”
- “131548 elements have missing property definitions.”

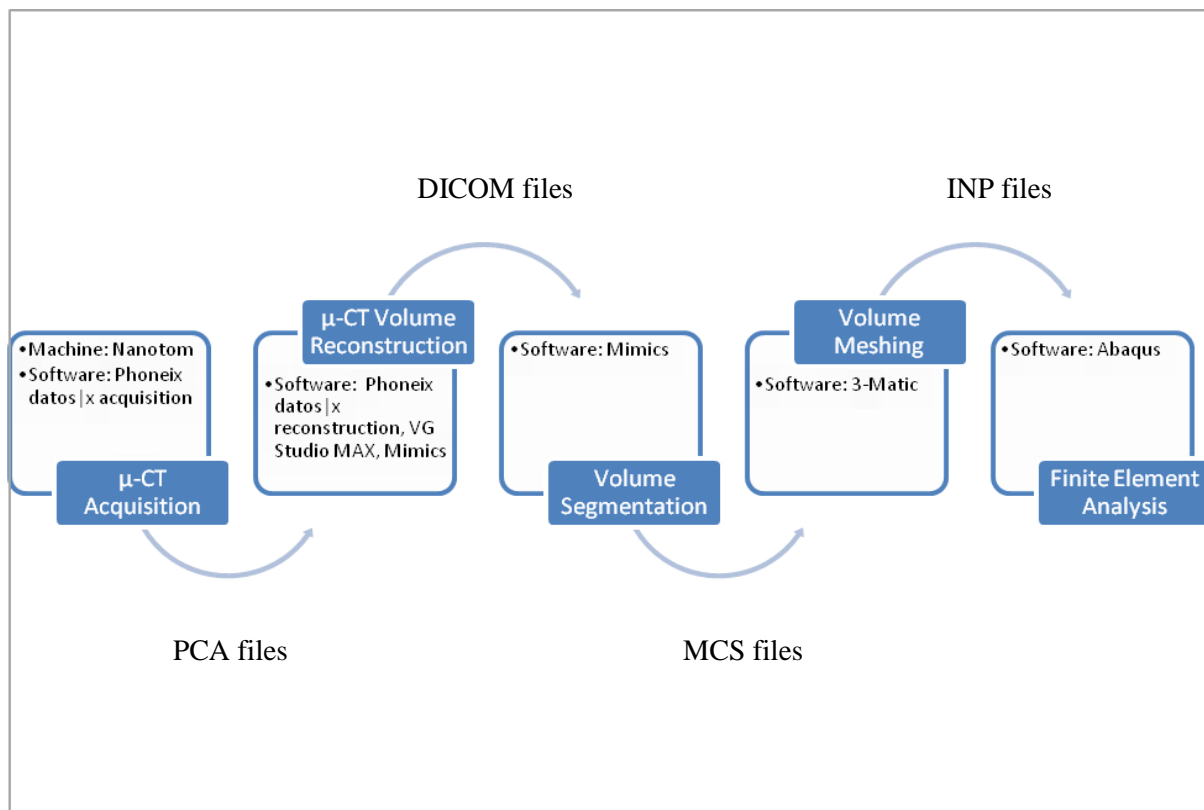


Figure 13. Flow chart of μ-CT to FEA protocol used with the file types obtained at each step.

## 4.2 FEA of Screw in Woven Bone

Finite element models of a magnesium alloy screw and a copolymer screw in bone were created to obtain preliminary results of the screws' behavior in new/woven bone. A screw-in-bone model, created by Hawkins (Hawkins, 2013), was successfully used to perform this analysis.

**4.2.1 Meshing.** Upon meshing, the following warning was received: "Some of the mid-edge nodes were not projected onto the geometric boundary, in order to avoid forming bad elements." The numbers of surface and volume elements generated on the model by the 0.0015 seed size were 10,430 and 64,633 respectively. A global seed size of 0.001 produces over 100,000 elements, which is the quota of the academic license. A global seed size of 0.0013 gave 99,465 volume elements. Abaqus was not able to complete a mesh with a global seed size of 0.002. It was not fine enough for the edge of the screw's revolutions to be meshed.

**4.2.2 Output.** The reaction forces are assumed to be the equal but opposite force acting on the bone as the screw is removed from the bone. The maximum reaction forces caused by the axial pull-out tests of a magnesium-alloy and a 82:18 PLLA:PLGA copolymer were obtained from the finite element analysis results of both material types in woven bone of a minimum and maximum elastic modulus. The copolymer caused a greater reaction force magnitude in woven bone with maximum elastic modulus and greater reaction force in the vertical direction in woven bone with maximum elastic modulus than of the Mg-alloy in same (Table 7; figure 12). Comparison of the translation in the models that were caused by the axial pull-out of the screw, showed the same maximum displacement/translation in the magnesium-alloy models as in the copolymer models in woven bone of the same properties (Table 8; Figure13). Comparison of the

magnitude of the translation and the translation in the vertical direction (UT2) in each model only varied slightly (Figure 14).

Table 7

*Maximum reaction force values obtained from FEA of each model*

Model	Maximum force (N)			
	Magnitude, RF	Node	In Vertical Direction, RF2	Node
<b>Mg-alloy in <math>E_{\max}</math> Woven bone</b>	1.31377	47090	1.18333	91
<b>Mg-alloy in <math>E_{\min}</math> Woven bone</b>	0.0443	47090	0.0275	91
<b>Copolymer in <math>E_{\max}</math> Woven bone</b>	1.48443	91	1.48443	91
<b>Copolymer in <math>E_{\min}</math> Woven bone</b>	0.0283	47090	0.0283	91

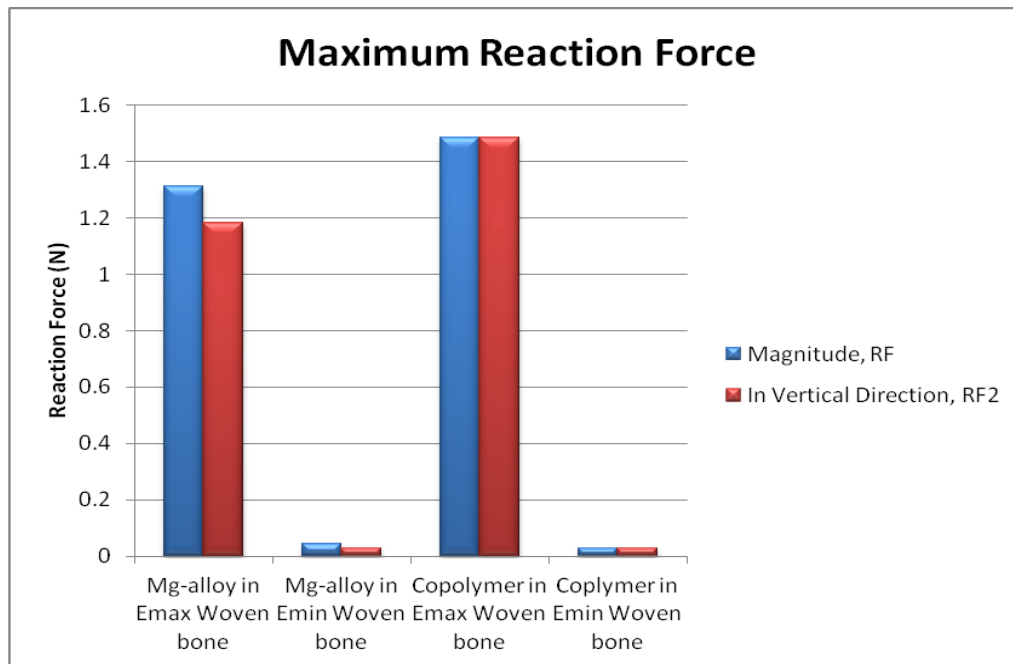


Figure 14. Bar chart of the maximum reaction force results of the FEA models.

Table 8

Maximum displacement values obtained from FEA of each model.

Model	Maximum displacement (m)			
	Magnitude, UT	Node	In Vertical Direction, UT2	Node
Mg-alloy in $E_{\max}$ Woven bone	3.00E-05	408	3.00E-05	29813
Mg-alloy in $E_{\min}$ Woven bone	3.00E-05	21540	3.00E-05	29813
Copolymer in $E_{\max}$ Woven bone	3.00E-05	411	3.00E-05	18767
Copolymer in $E_{\min}$ Woven bone	3.00E-05	408	3.00E-05	29813

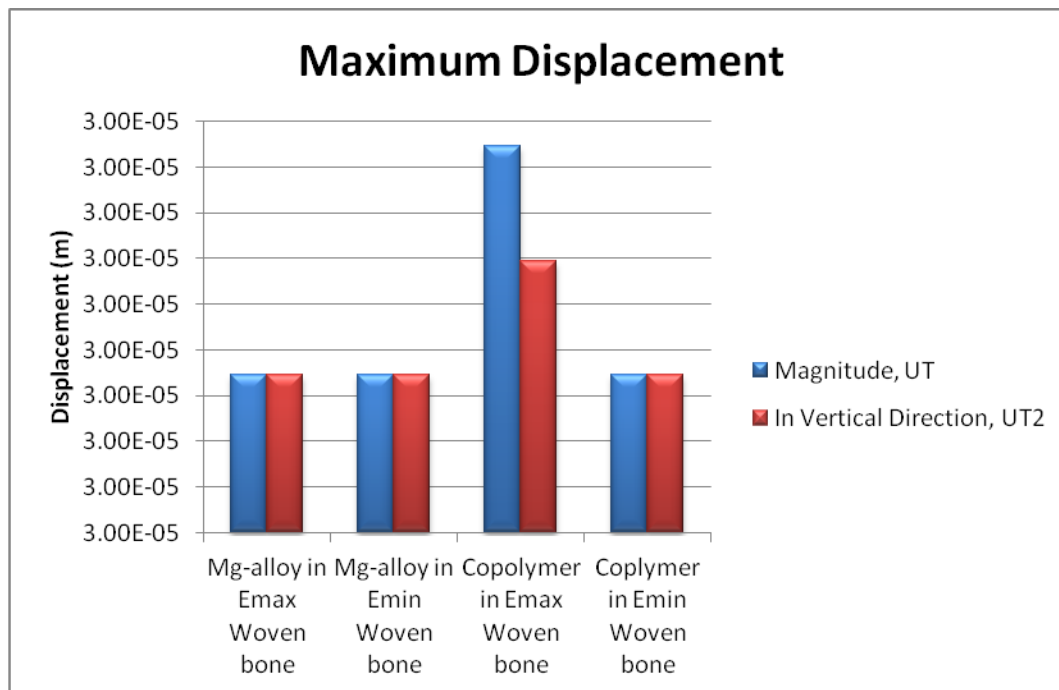


Figure 15. Bar chart of the maximum displacement results of the FEA models.

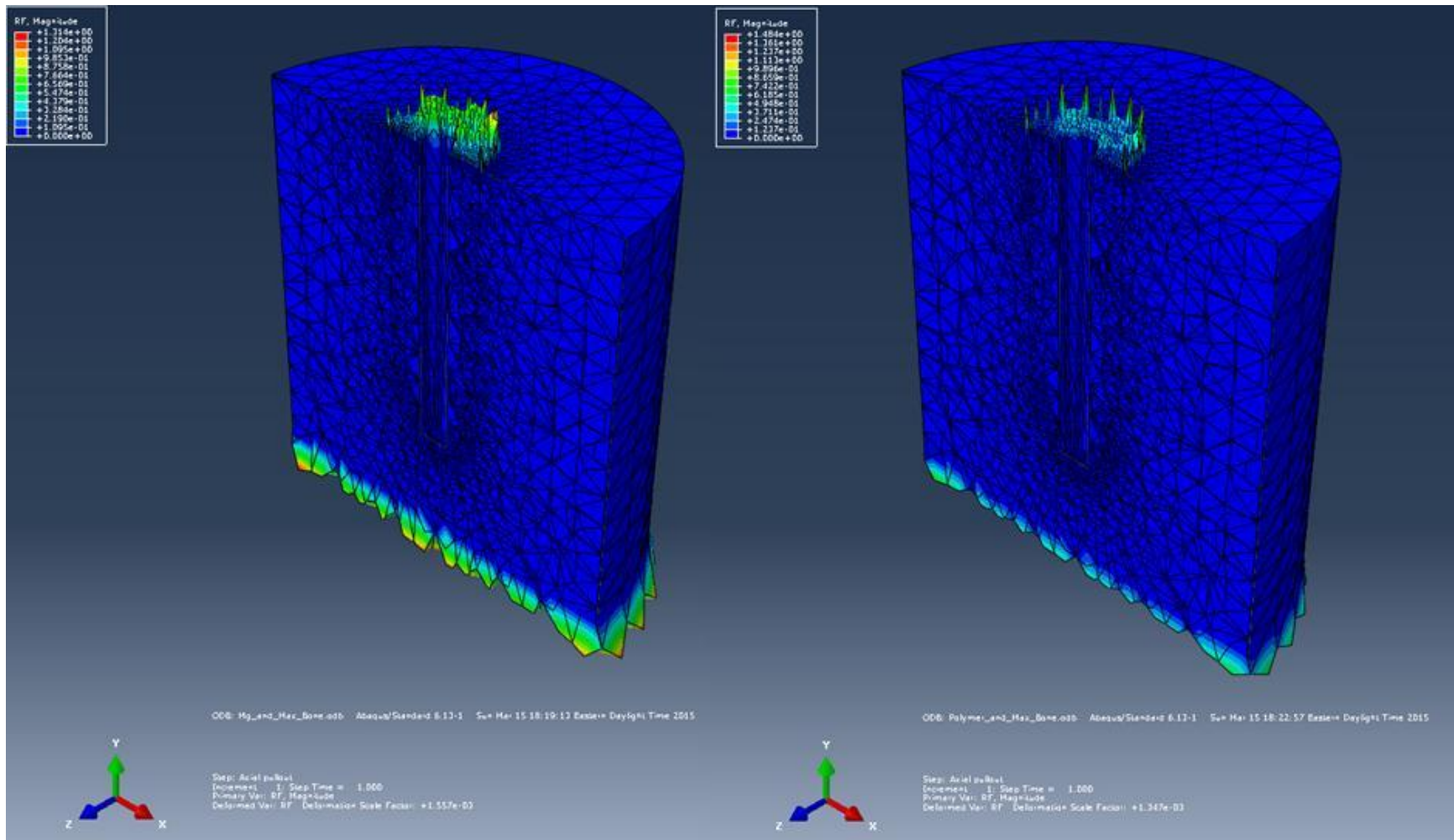


Figure 16. Comparison of the magnitudes of the reaction forces (RF) that occurred when the magnesium-alloy (left) and the PLLA:PLGA copolymer (right) underwent the same axial pull-out test in woven bone with a maximum elastic modulus.

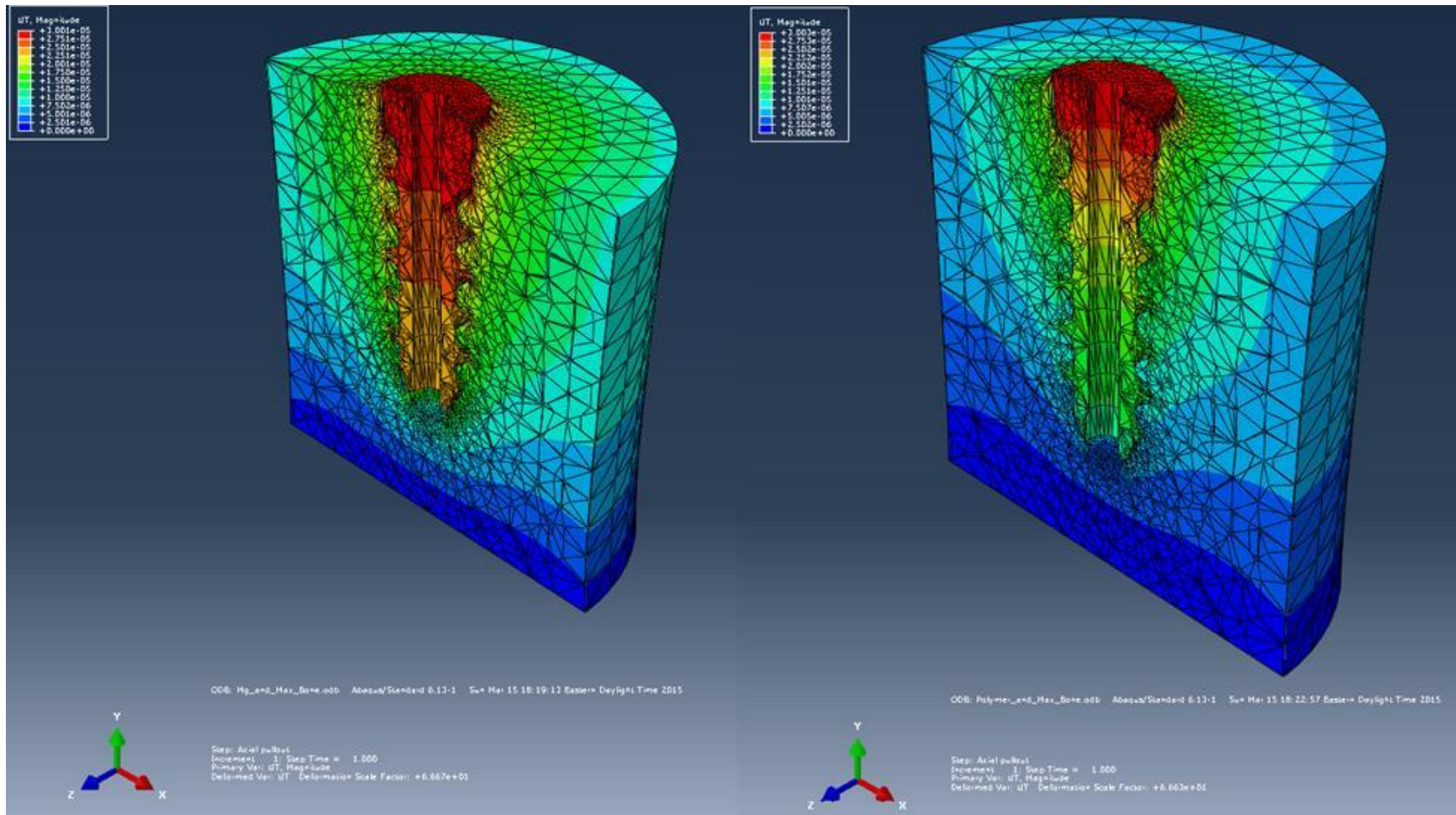


Figure 17. Comparison of the translation (UT) that occurred when the magnesium-alloy (left) and the PLLA:PLGA copolymer (right) underwent the same axial pull-out test in woven bone with a maximum elastic modulus.

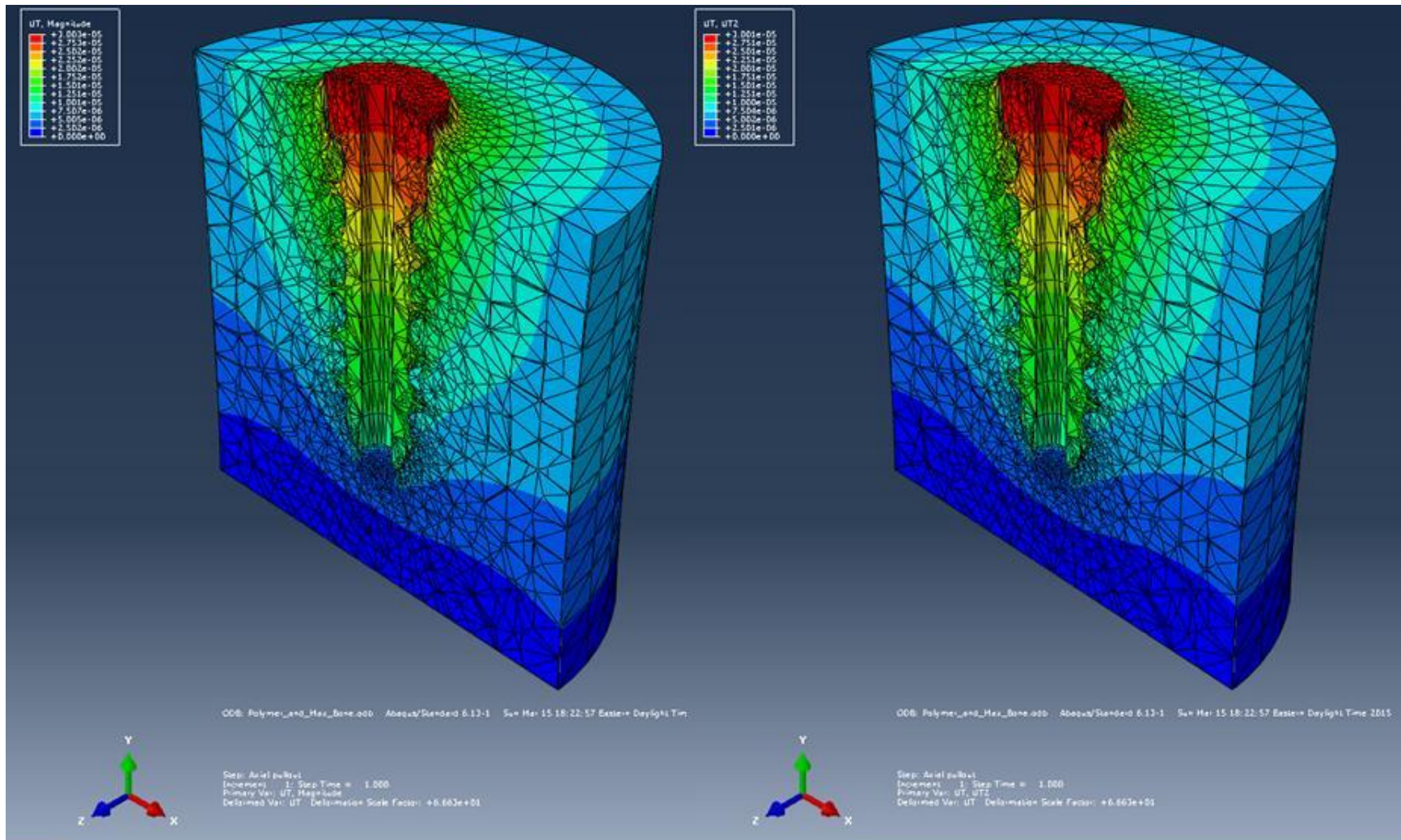


Figure 18. Comparison of the translation magnitude (UT) and the translation in the vertical direction (UT2) that occurred when the PLLA:PLGA copolymer (left and right) underwent pull-out testing in woven bone with a maximum elastic modulus.

## CHAPTER 5

### Discussion and Future Research

Given the need to develop more accurate finite element models of degrading magnesium/magnesium alloys, this study was designed to evaluate the CT to FEA process using CT scans of devices in bone. A second portion of the study was aimed at learning more about the mechanical properties of woven bone, for which there is little existing knowledge of its mechanical properties. Finally, this study enabled the comparison of pullout behavior of an unnamed magnesium alloy and a copolymer in woven bone. The hypothesis of this study was that the pull-out strength and displacement of an unnamed Mg-alloy screw would be higher than that of a 82:18 PLLA:PLGA copolymer screw.

#### 5.1 Micro-CT to Finite Element Analysis

**5.1.1 3-D volume segmentation.** The inclusion of outside pixels in masks could be due to insensitivity of Mimics at the high resolution given by micro-CT as opposed to clinical CT or simply due to the range of densities across the samples. The x-ray attenuation properties of magnesium are similar to bone. This may be why attenuation by thresholding of the Mg screw implant gave lots of extra voxels in the bone areas when the scans were being separated into different ‘masks’. This caused the separation to be done manually. General mask ranges exist in Mimics for different biological tissue such as adult and child cortical and cancellous bone. These pre-existing ranges are supposed to make the thresholding process easier and less time consuming. In this study, the pre-set values for human bone could not be used, because the data came from an animal study.

**5.1.2 Material property assignment.** Previous CT to FEA models of a metallic implant in bone have generated the bone CT data first, then simply added a drawing of the implant in or onto the bone with Boolean operations (Kluess, 2010). This achieves two things. First, it eliminates the problem of separating the geometry and thresholding, which may be imprecise. Secondly, it allows automatic material property assignment to bone using currently built software like BONEMAT (Fulvia Taddei, Pancanti, & Viceconti, 2004) before the implant is introduced.

The long-term goal of CT to FEA in this research is to use CT values or Hounsfield Units to directly translate the material properties to the geometry. However no equations or programs are available for rabbit bone though there are for human bone. One study presented an equation for the elastic modulus for rabbit cortical bone (Chen, Hsu, & Chang, 2003), but this could not input into Mimics' preset equation sections and cortical bone values was no use when cancellous/new bone was needed. Therefore the existing auto-mapping programs could not be used. There is also no mathematical model for mapping the properties of corrosion or degradation properties of magnesium onto the geometry of degrading devices, using CT data. The material properties of degradation and corrosion products of magnesium biomaterials need to be characterized.

### **5.1.3 Meshing in Mimics and 3-Matic**

**5.1.3.1 Meshing in Mimics.** Mimics allows manual selection of either a linear tetrahedral or hexahedra mesh. Apart from smoothing and volume compensation, Mimics enables voxel grouping by changing the XY and Z resolutions of the CT data. This reduces the number of elements and nodes in the model by grouping voxels together and assigning them the same properties. This is why the resulting meshes looked rough and pixelated and why the material

property histogram was not a smooth or continuous curve. Resolution of mesh could be decreased to a number of elements that could be processed but the mesh became very rough and grooves of the parts being meshed became unrecognizable for smaller parts, especially when hexahedral elements were used.

**5.1.3.2 Meshing in 3-Matic.** 3-Matic is Mimics' remesher. Remeshing in 3-Matic automatically increases and optimizes the quality of the triangles. Sharp edges may cause unwanted stress risers in finite element analysis, so smoothing and optimizing triangle quality reduces this effect. Reducing the number of triangles speeds up the FEA calculations. Once FEA meshes are created, Mimics can assign material properties based on Hounsfield units and export to FEA packages directly. 3-Matic has a quality preserving reduce mesh function, which may have been useful for the bone but was not needed for smaller parts like the Ti wires, screw and corrosion products.

Overall, meshing bone in 3-Matic needed too many elements for larger parts such as the bone and crashed program. Therefore the bone had to be meshed in Mimics where mesh resolution could be decreased enough to complete the model. Quadratic or higher order elements are preferred because they reduce the error for the solutions in FEA. However linear elements are often used when time and computing resources are limited.

**5.1.4 Finite Element Analysis.** Neither Abaqus nor SolidWorks were able to detect the geometry of files exported from the Mimics suite. The INP files open as models in Abaqus and not parts, which indicates that at the point for importing the files, the models only need boundary and load conditions before a job can be created and submitted. This would be because the models would already be meshed and assigned material properties.

## 5.2 FEA of Screw in Woven Bone

**5.2.1 Model creation.** Finite element models of a magnesium alloy screw and a copolymer screw in bone were created to obtain preliminary results of the screws' behavior in new/woven bone. The models used in this study, with the screw fitted directly into the bone block and no spaces at the interface, may not always occur during insertion of such devices *in vivo*. However, in press-fit implantation, the osteomy is created with a drill bit that is slightly smaller than or at most equal than the screw, so that all the spaces at the implant site are filled. Therefore the model is adequate for representing a press-fit implant.

**5.2.2 Meshing.** The elements used to mesh these models were automatically generated quadratic tetrahedral elements. These were the only types of elements that could mesh the complex geometries of the bone cavity and the screw. The mesh seed sizes of 0.0013-0.0015 were the narrow window that meshed the model within the 100,000 element quota of the Abaqus teaching license. The error message, "some of the mid-edge nodes were not projected onto the geometric boundary, in order to avoid forming bad elements," seen during meshing, was caused by the numerous small curvatures at the edges that were being meshed with elements that were too large.

The numbers of surface and volume elements generated on the model by the 0.0015 seed size were 10,430 and 64,633 respectively. A global seed size of 0.001 produces over 100,000 elements, which is the quota of the academic license. Abaqus was not able to complete a mesh of the edges when a global seed size of 0.002 was selected. So that seed size was not fine enough for the edge of the screw's revolutions to be meshed.

**5.2.3 Analysis and Output.** A quasi-static load means that the load is applied so slowly that the structure deforms very slowly (very low strain rate) resulting in a small inertial force that

can be ignored. Therefore a quasi-static analysis is one in which quasi-static forces are applied in the model, as with this study.

The maximum reaction forces in the bone for both models, occurred at the bottom of the bone, where it was constrained. The magnitude of the translation in the screws increased from the tip of the screw to the head. When compared, the magnesium alloy had higher reaction in forces in  $E_{\min}$  bone only and greater translation than the copolymer, indicating that the magnesium alloy had greater pull-out strength in the  $E_{\min}$  bone only. This partially agrees with previous research (A. Weiler, Windhagen, Raschke, Laumeier, & Hoffmann, 1998).

### **5.3 Limitations**

There were several resource limitations in this study. The CAD (SolidWorks) and CAE (Abaqus) software used in this study were teaching licenses and were limited in the work that it may be produced. A research edition of Abaqus may have been able to generate a finer mesh on the complex curves of the screws and bone cavity and in turn may have yielded better FE results. The Mimics license was either limited or required more RAM and processing speed than was available for processing the meshes of larger parts of the models such as bone and for generating finer meshes, especially at the curves and edges. As it was a first study, the computer used was not specific to the task and limited the meshes generated.

For the material properties, limitations existed in the values for woven bone. The nanoindentation values may be used for elastic moduli, but no density or Poisson's ratio values have been published for new bone. This form of osseous tissue is difficult to characterize and very little information is available about its material properties and there was no physical testing for this first model.

## 5.4 Future Work

More work needs to be done on automatic material property assignment to CT based models that are not solely host tissue or device, but a combination of both. The work is important because it is leading towards a degradation model of magnesium implants over time, which is essential for their clinical success.

The results of the finite element analysis of orthopedic devices in woven bone yielded small force values and more work needs to be done to determine the reason for these results and whether or not the results are realistic.

## 5.5 Conclusions

This study has thoroughly investigated the creation of finite element models of an orthopedic device *in vivo*, from computed tomography scans of the bones with the implanted device, as opposed to CT scans of the bone only and the superimposition of the device into the bone. Finite element models of an orthopedic device *in vivo*, from computed tomography scans of the bones with the implanted device, can be used to accurately model biodegradable magnesium over time. However these models require much more calibration of the CT system to account for the differences in material properties of biological tissue and orthopedic biomaterials and their effects on x-ray attenuation, which affects the accuracy material property mapping for FE models.

The results of this work have also shown that an unnamed biodegradable magnesium-alloy and a biodegradable 82:18 PLLA:PLGA copolymer performed equally in nodal displacement and the Mg-based device only outperformed the copolymer in  $E_{\min}$  woven bone. Therefore, these results neither proved nor disproved the hypothesis and they do not support the

existing studies that have proved that degradable magnesium screws are stronger polymer screws.

## References

- Al-Sanabani, J. S., Madfa, A. A., & Al-Sanabani, F. A. (2013). Application of calcium phosphate materials in dentistry. *Int J Biomater*, 2013, 876132. doi: 10.1155/2013/876132
- Almarza, A. J., Holmes, J. A., Chung, W. L., & Henderson, S. E. (2014). Biodegradable, magnesium-containing bone screws, methods for their preparation and medical applications therefor: Google Patents.
- Bartel, D. L., Davy, D. T., & Keaveny, T. M. (2006). *Orthopaedic Biomechanics: Mechanics and Design in Musculoskeletal Systems*: Pearson/Prentice Hall.
- Black, J. T., & Kohser, R. A. (2007). *DeGarmo's Materials and Processes in Manufacturing* (10th ed.): Wiley.
- Castellani, C., Lindtner, R. A., Hausbrandt, P., Tschegg, E., Stanzl-Tschegg, S. E., Zanoni, G., . . . Weinberg, A.-M. (2011). Bone–implant interface strength and osseointegration: Biodegradable magnesium alloy versus standard titanium control. *Acta Biomaterialia*, 7(1), 432-440. doi: <http://dx.doi.org/10.1016/j.actbio.2010.08.020>
- Chaffin, D. B., Andersson, G. B. J., & Martin, B. J. (2006). *Occupational Biomechanics*: Wiley.
- Chapman, J. R., Harrington, R. M., Lee, K. M., Anderson, P. A., Tencer, A. F., & Kowalski, D. (1996). Factors affecting the pullout strength of cancellous bone screws. *J Biomech Eng*, 118(3), 391-398.
- Chatzistergos, P. E., Magnissalis, E. A., & Kourkoulis, S. K. (2010). A parametric study of cylindrical pedicle screw design implications on the pullout performance using an experimentally validated finite-element model. *Medical Engineering & Physics*, 32(2), 145-154. doi: <http://dx.doi.org/10.1016/j.medengphy.2009.11.003>

- Chen, W. P., Hsu, J. T., & Chang, C. H. (2003). Determination of young's modulus of cortical bone directly from computed tomography: A rabbit model. *Journal of the Chinese Institute of Engineers*, 26(6), 737-745. doi: 10.1080/02533839.2003.9670828
- Christensen, F. B., Dalstra, M., Sejling, F., Overgaard, S., & Bunger, C. (2000). Titanium-alloy enhances bone-pedicle screw fixation: mechanical and histomorphometrical results of titanium-alloy versus stainless steel. *Eur Spine J*, 9(2), 97-103.
- Cody, D. D., Gross, G. J., J. Hou, F., Spencer, H. J., Goldstein, S. A., & P. Fyhrie, D. (1999). Femoral strength is better predicted by finite element models than QCT and DXA. *J Biomech*, 32(10), 1013-1020. doi: [http://dx.doi.org/10.1016/S0021-9290\(99\)00099-8](http://dx.doi.org/10.1016/S0021-9290(99)00099-8)
- Corporation, S. (2013). Physical Property Testing Equipment for Biomaterials and Medical Applications. In S. Corporation (Ed.). Japan.
- Eglin, D., & Alini, M. (2008). Degradable polymeric materials for osteosynthesis: tutorial. *Eur Cell Mater*, 16, 80-91.
- Erdmann, N., Angrisani, N., Reifenrath, J., Lucas, A., Thorey, F., Bormann, D., & Meyer-Lindenberg, A. (2011). Biomechanical testing and degradation analysis of MgCa0.8 alloy screws: A comparative in vivo study in rabbits. *Acta Biomaterialia*, 7(3), 1421-1428. doi: <http://dx.doi.org/10.1016/j.actbio.2010.10.031>
- Faulkner, K. G., Cann, C. E., & Hasegawa, B. H. (1991). Effect of bone distribution on vertebral strength: assessment with patient-specific nonlinear finite element analysis. *Radiology*, 179(3), 669-674. doi: 10.1148/radiology.179.3.2027972
- Feldman, K. A. (2005). The Principles of Interference Screw Fixation: Application to Foot and Ankle Surgery. *The Journal of Foot and Ankle Surgery*, 44(6), 455-461. doi: <http://dx.doi.org/10.1053/j.jfas.2005.07.024>

- Gaweda, K., Walawski, J., Weglowski, R., & Krzyzanowski, W. (2009). Comparison of bioabsorbable interference screws and posts for distal fixation in anterior cruciate ligament reconstruction. *Int Orthop*, 33(1), 123-127. doi: 10.1007/s00264-007-0482-y
- Hawkins, K. M. (2013). Parametric Finite Element Analysis of Magnesium Based Anterior Cruciate Ligament Interference Screws For the Purpose of Optimizing Screw Purchase.
- Henderson, S. E., Verdelis, K., Maiti, S., Pal, S., Chung, W. L., Chou, D.-T., . . . Almarza, A. J. (2014). Magnesium alloys as a biomaterial for degradable craniofacial screws. *Acta Biomaterialia*, 10(5), 2323-2332. doi: <http://dx.doi.org/10.1016/j.actbio.2013.12.040>
- Herrera, A., Ibarz, E., Cegonino, J., Lobo-Escolar, A., Puertolas, S., Lopez, E., . . . Gracia, L. (2012). Applications of finite element simulation in orthopedic and trauma surgery. *World J Orthop*, 3(4), 25-41. doi: 10.5312/wjo.v3.i4.25
- Hou, S. M., Hsu, C. C., Wang, J. L., Chao, C. K., & Lin, J. (2004). Mechanical tests and finite element models for bone holding power of tibial locking screws. *Clin Biomech (Bristol, Avon)*, 19(7), 738-745. doi: 10.1016/j.clinbiomech.2004.04.012
- Jacobs, J. J., Hallab, N. J., Skipor, A. K., & Urban, R. M. (2003). Metal degradation products: a cause for concern in metal-metal bearings? *Clin Orthop Relat Res*(417), 139-147. doi: 10.1097/01.blo.0000096810.78689.62
- Jamshidian, M., Tehrany, E. A., Imran, M., Jacquot, M., & Desobry, S. (2010). Poly-Lactic Acid: Production, Applications, Nanocomposites, and Release Studies. *Comprehensive Reviews in Food Science and Food Safety*, 9(5), 552-571. doi: 10.1111/j.1541-4337.2010.00126.x
- Keaveny, T. M., Morgan, E. F., & Yeh, O. C. (2003). Bone Mechanics. In M. Kutz (Ed.), *Standard Handbook of Biomedical Engineering and Design* (pp. 8.1-8.23): McGraw-Hill.

- Keyak, J. H., Meagher, J. M., Skinner, H. B., & Mote Jr, C. D. (1990). Automated three-dimensional finite element modelling of bone: a new method. *Journal of Biomedical Engineering*, 12(5), 389-397. doi: [http://dx.doi.org/10.1016/0141-5425\(90\)90022-F](http://dx.doi.org/10.1016/0141-5425(90)90022-F)
- Keyak, J. H., Rossi, S. A., Jones, K. A., Les, C. M., & Skinner, H. B. (2001). Prediction of fracture location in the proximal femur using finite element models. *Medical Engineering & Physics*, 23(9), 657-664. doi: [http://dx.doi.org/10.1016/S1350-4533\(01\)00094-7](http://dx.doi.org/10.1016/S1350-4533(01)00094-7)
- Keyak, J. H., Rossi, S. A., Jones, K. A., & Skinner, H. B. (1997). Prediction of femoral fracture load using automated finite element modeling. *J Biomech*, 31(2), 125-133. doi: [http://dx.doi.org/10.1016/S0021-9290\(97\)00123-1](http://dx.doi.org/10.1016/S0021-9290(97)00123-1)
- Kim, S. M., Jo, J. H., Lee, S. M., Kang, M. H., Kim, H. E., Estrin, Y., . . . Koh, Y. H. (2014). Hydroxyapatite-coated magnesium implants with improved in vitro and in vivo biocorrosion, biocompatibility, and bone response. *J Biomed Mater Res A*, 102(2), 429-441. doi: 10.1002/jbm.a.34718
- Klues, D. (2010). Finite Element Analysis in Orthopaedic Biomechanics. In D. Moratal (Ed.), *Finite Element Analysis* (pp. 151-170). Croatia: InTech.
- Leong, P. L., & Morgan, E. F. (2008). Measurement of fracture callus material properties via nanoindentation. *Acta Biomaterialia*, 4(5), 1569-1575. doi: <http://dx.doi.org/10.1016/j.actbio.2008.02.030>
- Lian, K. C., Lang, T. F., Keyak, J. H., Modin, G. W., Rehman, Q., Do, L., & Lane, N. E. (2005). Differences in hip quantitative computed tomography (QCT) measurements of bone mineral density and bone strength between glucocorticoid-treated and glucocorticoid-naive postmenopausal women. *Osteoporos Int*, 16(6), 642-650. doi: 10.1007/s00198-004-1736-9

- McCloskey, C., & Furnival, T. (2011). Structure and composition of bone. Retrieved March 11, 2015, from <http://www.doitpoms.ac.uk/tlplib/bones/structure.php>
- Morgan, D. G. (2015). Knee Conditions. Retrieved March 11, 2015, from <http://www.drdauidmorgan.com.au/knee-conditions#top>
- Morgan, E. F., & Bouxsein, M. L. (2005). Use of finite element analysis to assess bone strength. *IBMS BoneKEy*, 2(12), 8-19.
- Ogele, T. A. (2013). BoneOpenStax CNX. Retrieved from <http://cnx.org/contents/18898be3-14fc-472b-bc96-45e5a94998cd@1/Bone>.
- Okuma, T. (2001). Magnesium and bone strength. *Nutrition*, 17(7–8), 679-680. doi: [http://dx.doi.org/10.1016/S0899-9007\(01\)00551-2](http://dx.doi.org/10.1016/S0899-9007(01)00551-2)
- Park, J. B., & Bronzino, J. D. (2002). *Biomaterials: Principles and Applications*: CRC Press.
- Parmar, A. (2014, January 30, 2014). Global Market for Orthopedics Devices to Grow to \$41.2 B by 2019. Retrieved March 5, 2015, from <http://www.mddionline.com/article/global-market-orthopedics-devices-grow-412-b-2019>
- Pietrzak, W. S., Caminear, D. S., & Perns, S. V. (2002). Mechanical characteristics of an absorbable copolymer internal fixation pin. *J Foot Ankle Surg*, 41(6), 379-388.
- Pistoia, W., van Rietbergen, B., Lochmüller, E. M., Lill, C. A., Eckstein, F., & Rügsegger, P. (2002). Estimation of distal radius failure load with micro-finite element analysis models based on three-dimensional peripheral quantitative computed tomography images. *Bone*, 30(6), 842-848. doi: [http://dx.doi.org/10.1016/S8756-3282\(02\)00736-6](http://dx.doi.org/10.1016/S8756-3282(02)00736-6)
- Salahinejad, E., Hadianfard, M. J., Macdonald, D. D., Sharifi Asl, S., Mozafari, M., Walker, K. J., . . . Tayebi, L. (2013). Surface modification of stainless steel orthopedic implants by sol-gel ZrTiO<sub>4</sub> and ZrTiO<sub>4</sub>-PMMA coatings. *J Biomed Nanotechnol*, 9(8), 1327-1335.

Schmitt, C. C., Elings, J. R., & Serry, M. (2010). Nanoindenting, Scratching and Wear Testing with the Atomic Force Microscope. In Bruker (Ed.).

Sharma, S. K., Sehgal, N., & Kumar, A. (2003). Biomolecules for development of biosensors and their applications. *Current Applied Physics*, 3(2–3), 307-316. doi: [http://dx.doi.org/10.1016/S1567-1739\(02\)00219-5](http://dx.doi.org/10.1016/S1567-1739(02)00219-5)

Staiger, M. P., Pietak, A. M., Huadmai, J., & Dias, G. (2006). Magnesium and its alloys as orthopedic biomaterials: A review. *Biomaterials*, 27(9), 1728-1734. doi: <http://dx.doi.org/10.1016/j.biomaterials.2005.10.003>

Taddei, F., Cristofolini, L., Martelli, S., Gill, H. S., & Viceconti, M. (2006). Subject-specific finite element models of long bones: An in vitro evaluation of the overall accuracy. *J Biomech*, 39(13), 2457-2467. doi: <http://dx.doi.org/10.1016/j.jbiomech.2005.07.018>

Taddei, F., Martelli, S., Reggiani, B., Cristofolini, L., & Viceconti, M. (2006). Finite-element modeling of bones from CT data: sensitivity to geometry and material uncertainties. *IEEE Trans Biomed Eng*, 53(11), 2194-2200. doi: 10.1109/tbme.2006.879473

Taddei, F., Pancanti, A., & Viceconti, M. (2004). An improved method for the automatic mapping of computed tomography numbers onto finite element models. *Medical Engineering & Physics*, 26(1), 61-69. doi: [http://dx.doi.org/10.1016/S1350-4533\(03\)00138-3](http://dx.doi.org/10.1016/S1350-4533(03)00138-3)

Ulrich, D., van Rietbergen, B., Laib, A., & R uegsegger, P. (1999). Load transfer analysis of the distal radius from in-vivo high-resolution CT-imaging. *J Biomech*, 32(8), 821-828. doi: [http://dx.doi.org/10.1016/S0021-9290\(99\)00062-7](http://dx.doi.org/10.1016/S0021-9290(99)00062-7)

van Rietbergen, B., Weinans, H., Huiskes, R., & Odgaard, A. (1995). A new method to determine trabecular bone elastic properties and loading using micromechanical finite-

- element models. *J Biomech*, 28(1), 69-81. doi: [http://dx.doi.org/10.1016/0021-9290\(95\)80008-5](http://dx.doi.org/10.1016/0021-9290(95)80008-5)
- Viceconti, M., Davinelli, M., Taddei, F., & Cappello, A. (2004). Automatic generation of accurate subject-specific bone finite element models to be used in clinical studies. *J Biomech*, 37(10), 1597-1605. doi: <http://dx.doi.org/10.1016/j.jbiomech.2003.12.030>
- Weiler, A., Peine, R., Pashmineh-Azar, A., Abel, C., Südkamp, N. P., & Hoffmann, R. F. G. (2002). Tendon healing in a bone tunnel. Part I: Biomechanical results after biodegradable interference fit fixation in a model of anterior cruciate ligament reconstruction in sheep. *Arthroscopy: The Journal of Arthroscopic & Related Surgery*, 18(2), 113-123. doi: <http://dx.doi.org/10.1053/jars.2002.30656>
- Weiler, A., Windhagen, H. J., Raschke, M. J., Laumeyer, A., & Hoffmann, R. F. (1998). Biodegradable interference screw fixation exhibits pull-out force and stiffness similar to titanium screws. *Am J Sports Med*, 26(1), 119-126.
- Witte, F., Crostack, H.-A., J., N., & Beckmann, F. (2001). Characterization of degradable magnesium alloys as orthopaedic implant material by synchrotron-radiation-based microtomography.
- Witte, F., Fischer, J., Nellesen, J., Crostack, H.-A., Kaese, V., Pisch, A., . . . Windhagen, H. (2006). In vitro and in vivo corrosion measurements of magnesium alloys. *Biomaterials*, 27(7), 1013-1018. doi: <http://dx.doi.org/10.1016/j.biomaterials.2005.07.037>
- Witte, F., Kaese, V., Haferkamp, H., Switzer, E., Meyer-Lindenberg, A., Wirth, C. J., & Windhagen, H. (2005). In vivo corrosion of four magnesium alloys and the associated bone response. *Biomaterials*, 26(17), 3557-3563. doi: <http://dx.doi.org/10.1016/j.biomaterials.2004.09.049>

- Witte, F., Ulrich, H., Palm, C., & Willbold, E. (2007). Biodegradable magnesium scaffolds: Part II: Peri-implant bone remodeling. *Journal of Biomedical Materials Research Part A*, 81A(3), 757-765. doi: 10.1002/jbm.a.31293
- Wu, C., Ramaswamy, Y., Gale, D., Yang, W., Xiao, K., Zhang, L., . . . Zreiqat, H. (2008). Novel sphene coatings on Ti-6Al-4V for orthopedic implants using sol-gel method. *Acta Biomaterialia*, 4(3), 569-576. doi: <http://dx.doi.org/10.1016/j.actbio.2007.11.005>
- Zdero, R., Elfallah, K., Olsen, M., & Schemitsch, E. H. (2009). Cortical screw purchase in synthetic and human femurs. *J Biomech Eng*, 131(9), 094503. doi: 10.1115/1.3194755
- Zhang, E., Xu, L., Yu, G., Pan, F., & Yang, K. (2009). In vivo evaluation of biodegradable magnesium alloy bone implant in the first 6 months implantation. *Journal of Biomedical Materials Research Part A*, 90A(3), 882-893. doi: 10.1002/jbm.a.32132
- Zhao, Y., & Ovaert, T. C. (2010). Error Estimation of Nanoindentation Mechanical Properties Near a Dissimilar Interface via Finite Element Analysis and Analytical Solution Methods. *Journal of materials research*, 25(12), 2308-2316. doi: 10.1557/jmr.2010.0295